University of New Orleans
ScholarWorks@UNO

University of New Orleans Theses and Dissertations | Dissertations and Theses

Fall 12-20-2013

Rocket Motor Diagnostics using Tunable Diode Laser Spectroscopy for Chemically Non-Reacting Air/Water Vapor Mixture in Internal Flow

Wesley Carleton
wcarleto@uno.edu

Follow this and additional works at: https://scholarworks.uno.edu/td

 Part of the Mechanical Engineering Commons

Recommended Citation

Carleton, Wesley, "Rocket Motor Diagnostics using Tunable Diode Laser Spectroscopy for Chemically Non-Reacting Air/Water Vapor Mixture in Internal Flow" (2013). *University of New Orleans Theses and Dissertations*. 1729.
https://scholarworks.uno.edu/td/1729

This Thesis is protected by copyright and/or related rights. It has been brought to you by ScholarWorks@UNO with permission from the rights-holder(s). You are free to use this Thesis in any way that is permitted by the copyright and related rights legislation that applies to your use. For other uses you need to obtain permission from the rights-holder(s) directly, unless additional rights are indicated by a Creative Commons license in the record and/or on the work itself.

This Thesis has been accepted for inclusion in University of New Orleans Theses and Dissertations by an authorized administrator of ScholarWorks@UNO. For more information, please contact scholarworks@uno.edu.

Rocket Motor Diagnostics using Tunable Diode Laser Spectroscopy for Chemically Non-Reacting Air/Water Vapor Mixture in Internal Flow

A Thesis

Submitted to the Graduate Faculty of the

University of New Orleans

In partial fulfillment of the

Requirements for the degree of

Master of Science

In

Engineering

Mechanical Engineering

by

Wesley Carleton

B.S., University of Colorado at Colorado Springs, 2010

December 2013

Dedicated to my parents, Kim Campbell and Kurt Carleton

Acknowledgements

I would like to emphasize the contribution from my major professor Dr. K. Akyuzlu. Without his knowledge and mentorship this work could not be completed. I would also like to thank my committee members Dr. T. Wang, Dr. B. Taravella, Dr. Dr. D. Hui, and Dr. U. Chakravarty.

Additionally, I would like to thank Dr. StCyr for facilitating the donation of the TDLAS equipment and D. Coote from Stennis Space Center for donating this equipment to the UNO Combustion Lab. A. Fahrland was also instrumental in the operation and understanding of the TDLAS equipment and M. Chidurala was indispensible in the construction of the experimental setup.

Table of contents

List of Tables

List of Figures

Nomenclature

Symbols

A_c	cross sectional area
AR	channel aspect ratio (L/D)
C_f	friction coefficient
c_p	specific heat at constant pressure
D	diameter of the pipe
t	thickness of the pipe
F	frictional losses, shape factor
Iv	beam intensity
ν	wavelength
k	thermal conductivity
c	speed of light
l	path length
S(T)	line strength
N	number density
h	plancks constant
L	axial length of the channel
m	mass flow rate
n	Stoichiometric constant
p	pressure of the gas
Pr	Prandtl number
Ma	Mach number
q	heat flux
R	gas constant
Re	Reynolds number
T	time
T	temperature
u_x	axial velocity
r	radial coordinate
x	axial coordinate

Greek Symbols

ε	turbulence dissipation function, roughness factor
μ	absolute viscosity
ν	kinematic viscosity
ρ	density
τ	shear stress

Abstract

This research is for the implementation of non-intrusive measurement techniques in the study of high temperature pipe flow. A low pressure, laboratory scale hybrid rocket motor simulator was built to achieve high temperatures with various gases. A quartz test section was designed, built, and implemented into the existing test setup to accommodate the laser beam of the existing Tunable Diode Laser Absorption Spectrometer (TDLAS) system which was designed to observe water vapor. A super-heated water vapor injector was designed to obtain the desired water vapor concentrations. Flow characteristics were simultaneously recorded using the existing TDLAS system and the DAQ system for temperatures for later comparison. A numerical study using a commercial CFD package was used to predict the flow characteristics at certain locations for experimental comparison. Based on this study, it is concluded that the TDLAS can be used to make real time temperature measurements of heated internal gas flows.

Keywords: Tunable Diode Laser Absorption Spectroscopy, Water Vapor temperature measurements in the 1.4μm near infrared

Chapter 1

Introduction

Absorption spectroscopy has been around since the early 1970's for CO emission values in automobiles and industrial plants. Soon this technology was turned towards academic research in high-speed flow fields. Diode lasers became the main focus of absorption spectroscopy due to their robust nature, low cost, versatility, and ability to integrate with a fiber optic system. They are also able to achieve consistent measurements in harsh flow environments generally associated with turbulent chemically reacting flows.

Diode-laser absorption spectroscopy techniques have recently become of interest to a multitude of high-temperature combustion applications due to the technique's ability to capture parameters without affecting flow behavior. Studies have been performed on external flows simulating of PDE's, methane combustion, wind tunnels, etc.

The goal of this thesis is to adopt this technique in internal pipe flow where high temperatures and high velocities are experienced. Previous studies have not found any application of the measurement of temperature and density for internal flows. This will be achieved by measuring temperature, velocity and concentration of species of pipe flow using Plexiglas and quartz to limit optical disturbances. An experimental setup was built equipped to measure velocity, temperature, and density using pressure transducers and thermocouples upstream and downstream of the observation port to verify and calibrate the tunable diode laser system.

First, a literature survey was conducted to assess the range of applications and limitations of absorption spectroscopy. A thorough summary of successful techniques in various

applications is explained as well as a detailed discussion of the appropriate theory behind absorption spectroscopy. Next a description of the experimental setup and the governing techniques associated with the equipment is discussed. In chapter 5, a numerical study is described with the results to follow in Chapter 6 and Appendix A. Finally, the experimental results are examined and compared with intrusive measurement techniques and a 3D computational model.

Chapter 2

Literature Survey

There are a variety of non-intrusive measurement techniques for a wide range of applications. For simple temperature measurements, where thermocouples either cannot withstand the extreme temperatures or the exposure of the thermocouple to a sensitive system is too intrusive for accurate results, a non-intrusive measurement system is warranted. If temperature is the only parameter of interest, a pyrometer is often used to measure the irradiance of a medium by using the Stefan-Boltzmann law of radiation. Pyrometers have been used since the early 1900's and are still prevalent today. This technology is tried and true but is limited in its ability to measure temperature alone.

For measuring velocity there are several existing technologies that can measure the fluid flow non-intrusively. Laser Doppler Anemometry (LDA) has been around for a long time and uses the Doppler shift to measure the velocity of a fluid flow. The system requires seeded particles with roughly the same buoyancy and density as the medium being observed. The system consists of two beams, usually one beam split to ensure coherence, that cross at a point of interest in the fluid flow. Although proven to be accurate, the LDA can only observe the fluid locally where the beams cross one another.

The other predominant system used to measure velocity in a fluid flow is the Particle Image Velocimeter (PIV). The PIV is the successor of the LDA and can observe particles in a flow globally in 2 dimensions. This system requires seeded particles that very closely match the properties of the flow of interest otherwise they will not follow the behavior of the flow closely and results will be inaccurate. A laser is transmitted to the fluid and is scattered from the seeded

particles and a camera is used to capture the scattered light. The system is heavily reliant on a camera that has the ability to capture multiple frames at very high speeds. A highly synchronized system of lazing and digital capturing of the system is used to achieve an analysis that produces vectors and a time history of the particles movements. The drawbacks to this system are the requirement of seeded particles that closely match the medium of interest and the expense of the system itself with a costly high speed camera.

The third parameter of interest is concentration of species within a medium. A mass spectrometer has been useful in determining the concentration of a medium but is limited in its applications. The particles must first be ionized then after exposure to a predetermined electromagnetic field its radiation is measured to determine the matter associated with that specific electrical charge. This requires a long post processing time and limits the accuracy of an external flow due to the necessity to divert flow to be analyzed.

Finally absorption spectroscopy became of interest due to its versatility and advantages in a range of applications. Early conceptual experiments for combustion gases in-situ measurements were performed in the mid-infrared range [Arroyo et al, 1993 & 1994]. In the 1980's, it was demonstrated that high powered, tunable lasers could measure concentration of species, velocity, and temperature in combustion flow for 1, 2, and 3 dimensional geometries [Baer et al, 1994 & 2009]. Suddenly the prospect of measuring a variety of parameters with a single system sparked large interest among government, commercial, and academic research.

Early restrictions of absorption spectroscopy were due to the relatively weak diode lasers being produced at the time. Extremely weak power outputs of these lasers yielded complications with noise, beam distortion, difficulty in alignment, and low sensitivity for reacting and non-

reacting flows. However, due to the compact nature, cost, and reliability of diode lasers, research continued to solve these early problems.

It has been shown that using external cavity diode lasers could increase the accuracy of measuring combustion particles, H_20 & CO_2, in open flame combustion of C_2H_4 [Mihalcea et al, 1997 & 1998]. Due to the relatively weak vibrational overtones associated with spectral regions of commercially available tunable diode lasers in the .63-1.8 μm, high frequency wavelength modulation was developed to increase sensitivity.

One limitation that arose with absorption spectroscopy was the noise associated with combustion particles interfering with the wavelength of interest. A scanned wavelength approach utilizes ratios of integrated absorbance helps get around this issue [Zhou et al, 2005 & 2007]. Their research uses wavelength modulation with 2f detection to isolate the second harmonic of the initial transmitted frequency.

All of absorption spectroscopy can only be utilized if the line strength and corresponding rovibrational frequencies are known. An extensive research into the fundamental absorption characteristics of a given species was investigated and catalogued into the US Air Force HITRAN database [Veale et al, 1992].

For unique combustion particles of interest, studies have shown the technique for determining line position and line strengths in 1.63*nm* region [Chou et al, 1997]. They also showed how to determine the minimum detectable concentration of the observed medium required in this spectral region. They further demonstrated how to calibrate the diode lasers to determine critical line strengths [Chang et al, 2010].

Another way to ebb the noise due to combustion particles is to apply optical technology to the measurement system. [Allen et al, 2002] showed that refracting lenses can help separate combustion particles with similar frequencies to that of the transmitting laser. This was achieved by changing the angle of the beam as it leaves the transmitter and enters the detector in order to essentially filter out unwanted disturbances.

It has been demonstrated that using line-of-sight absorption techniques to measure non-uniform flows by scanning over broad wavelengths with vertical cavity surface-emitting lasers have successfully measured temperature and concentration of species [Furlong et al, 1998]. This showed that by extending the path length of the laser through the absorbing medium thus increasing the magnitude of absorption and limiting the possibility of disturbances improves accuracy [Liu et al, 2004 & 2007].

The versatility associated with diode lasers allows a practical way to achieve observation of a wide variety of molecules associated with all kinds of flows. Common molecules studied extensively include CO, O_2, H_20, CO_2 and CH_4.

Chapter 3

Experimental Setup

The following sections explain the theory associated with the experimental setup and equipment used for measuring temperature non-intrusively. Section 3.1 describes the basic theory and equations for absorption spectroscopy. Section 3.2 describes the operational theory of the TDLAS used in this research. The data acquisition system and experimental drawings are shown in section 3.3.

3.1 Theory of Absorption Spectroscopy

Absorption spectroscopy is based on the change in intensity correlated between the detector and diode laser across a medium of interest. The absorption is quantified by the Beer-Lambert relation:

$$I_v = I_{v,0} exp\left[-S(T)g(v-v_0)N\ell\right] \quad (1)$$

where I_v is the laser intensity, v is the frequency, l is the path length through the medium and N is the number density of the absorbing species. The strength of the absorption is determined by the temperature dependent line-strength $S(T)$, and the line shape function, $g(v - v_0)$ [Allen et al, 2002].

The line strength is determined by the temperature and pressure based line shape function. The line shape function describes the molecular transition frequency which broadens during collisional and thermal processes. Line strength is shown to be temperature dependent by Boltzmann's population statistics which defines the distribution of the internal energy-level of

the absorbing species. It has been shown from Baer et al that the line strength of the absorption transition is a fundamental spectroscopic property of the absorbing species. There are various databases that tabulate this spectral property for common atoms and molecules. The most extensive and commonly used database is provided by the US Air Force HITRAN database.

The line strength can be calculated from the known line strength at temperature $S(T_0)$using:

$$S(T) = S(T_0)\frac{Q(T_0)}{Q(T)}\exp\left[-\frac{hcE}{k}\left(\frac{1}{T}-\frac{1}{T_0}\right)\right]\times\left[\frac{1-\exp(-hcE/kT)}{1-\exp(-hcE/kT_0}\right] \quad (2)$$

where *Q* is the total molecular internal partition function, *E* is the energy of the lower transition state, *h* is Planck's constant, *k* is Boltzmann's constant and *c* is the speed of light. For near atmospheric pressure and the equipment used in this experiment, a Voigt profile that takes into account the frequency broadening due to thermal and collisional processes is used to describe the line shape function. Therefore with knowing or obtaining the line strength and line shape function, the change in intensity can be used to directly calculate the temperature of the observing species using the Beer-Lambert relation.

If the temperature of the gas is known, along with the line strength and absorption path, the number density of the absorbing species can be calculated by the measured transmission. One or two absorption transitions may be probed in order to determine number density. The ratio of absorbance of each transition is a pure function of temperature and calculated by:

$$R = \left(\frac{S_1}{S_2}\right)_{T_0} exp\left[\frac{-hc\Delta E}{k}\left(\frac{1}{T}-\frac{1}{T_0}\right)\right] \quad (3)$$

Where S_1 and S_2 are the line strength values at some reference temperature, $S(T_0)$, and ΔE is the energy separation of the absorbing states.

Lastly using the Doppler-shift, velocity of a given medium can be measured as the laser beam propagates across a flow field and calculated by:

$$\Delta v_{Doppler} = \frac{v}{c} v_0 cos\theta \tag{4}$$

where theta is the angle between the laser propagation and bulk flow directions. Two lasers separated by a given angle must be used to capture the shift in frequency between the two transmitting lasers.

When measuring small differences in intensity across combustion particles certain techniques have to be utilized in order to limit interference from beam steering and scattering due to refraction, combustion interference, soot and fuel spray that plagued early experiments of reacting flows. Several approaches are practiced to help overcome some of these difficulties. Wavelength modulation is used to minimize interference from emission and beam steering by scanning across the absorption profile continuously. The signal is then detected at a harmonic of the modulation frequency. The second form of wavelength modulation is to increase the lasing frequency in order to minimize noise and increase sensitivity.

Cavity modulation such as ECDL and VCSEL are two techniques used to decrease ambient noise by increasing the absorption length of the exposed medium. However this limits the application of the system and makes in-situ measuring of real world combustion flows not practical due to the necessity to divert flow to an external cavity.

Digital feedback lasers have been used extensively for their reliability and low cost. DFB lasers provide a precise and stable wavelength. Grating of the device controls diffraction and sends a constant wavelength output controlled by the initial grating. There are two ways to modify the fixed wavelength of DFB lasers. Providing heat or current to the DFB will change the grating through thermal expansion thus causing a measured change in the output wavelength. Altering the wavelength with temperature is relatively slow (a few Hz) due to thermal inertia and makes high frequency sampling difficult. The advantage is in its scanning capabilities in the 100cm-1 range. Applying current to the DFB can successfully manipulate the output frequency and make it sensitive to high frequency tuning up to 10GHz but a relatively narrow scanning capability of 1-2cm^{-1}.

3.2 Theory of Tunable Diode Laser Absorption Spectrometry

For the purpose of this equipment, there are 4 diode lasers that are tuned to 1343*nm*, 1388*nm*, 1392*nm*, and 1469*nm*. These wavelengths were chosen due to the low cost and availability of existing diode lasers tuned to these frequencies and the abundant information of the spectroscopic properties of water vapor at these wavelengths. This system uses distributed feedback lasers for their advantages described above. The equipment uses high frequency wavelength modulation at a rate of 10 kHz or greater to limit noise from combustion particles and the relatively weak absorption lines of water vapor associated with these wavelengths.

The four DFB lasers are combined into a single fiber optic cable and sampled at 2MHz. The four DFB lasers are scanned over the absorption features of interest by ramping the voltage to each laser. The results are a line-of-sight averaged reading of the medium of interest.

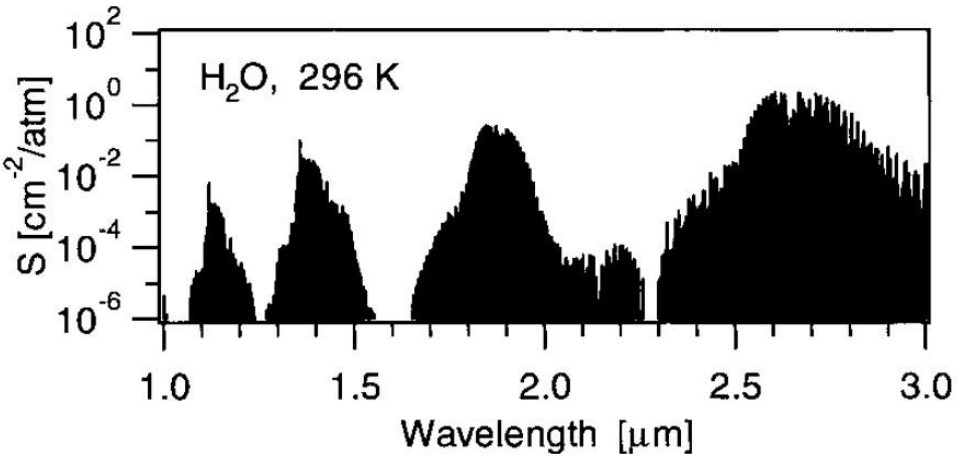

Figure 1- Absorption Spectra of Water Vapor at Room Temperature [Veale et al, 1992]

Figure 1 shows the multitude of absorption features in the near infrared spectrum. There are a variety of absorption lines to choose from depending on the temperatures of the desired application. Figure 2 shows the expanded view for the range of interest in this study which is in the 1.4μm region. Figure 3 shows the absorption lines chosen for the TDLAS equipment used in this study along with additional physical characteristics.

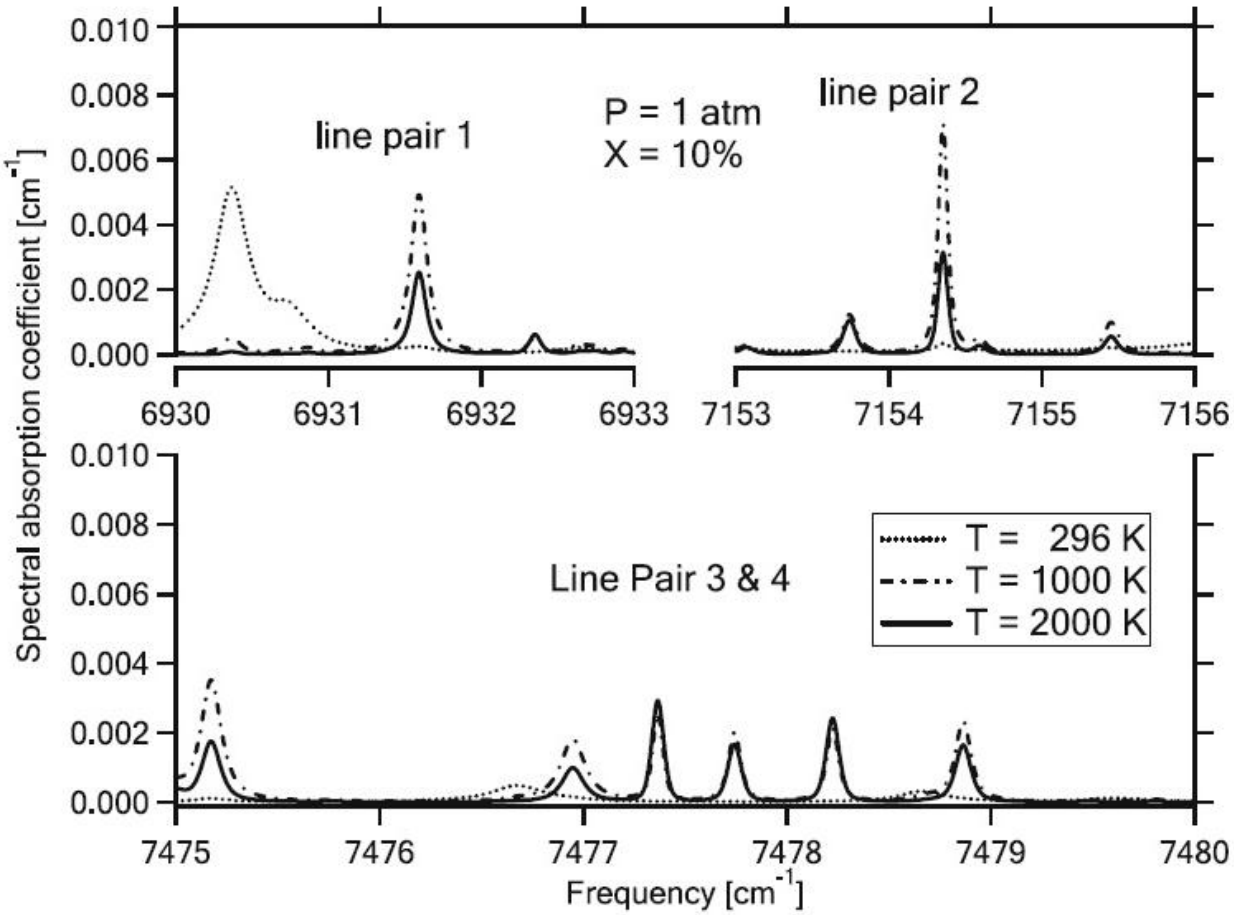

Figure 2 – Expanded View of Absorption Spectra for H_20 in the 1.4μm region from the HITRAN 2004 database for P= 1atm, 10% H_20, 90% air

Table 1 – Candidate $H_2 0$ line intensity pairs for temperature measurements between 1-2μm region from HITRAN2004

Line pair	λ [nm]	ν [cm^{-1}]	$10^3 S$ @1000 K [cm^{-2} atm^{-1}]	E'' [cm^{-1}]	$\Delta E''$ [cm^{-1}]	Max P^* [atm]	Line Spacing [cm^{-1}]	Notes
1	1442.67 1442.51	6931.592 6932.352	4.604E-4 4.604E-7	1813.22 3072.73	1259.73	2.2	0.760	B
2	1397.87 1397.75	7153.748 7154.354	5.504E-6 3.852E-4	2552.86 1789.04	763.82	3.7	0.606	B, E
3	1337.44 1337.37	7476.949 7477.366	1.421E-4 5.403E-7	1899.01 3319.45	1420.44	5.0	0.417	A, C, D
4	1337.44 1337.30	7476.949 7477.743	1.421E-4 3.954E-6	1899.01 2746.02	847.01	5.0	0.794	A, C, D
5	1982.87 1982.66	5043.193 5043.738	9.927E-7 9.267E-5	3058.40 2246.88	811.52	2.8	0.545	B
6	1981.83 1981.54	5045.831 5046.576	2.242E-6 5.554E-5	2915.89 2105.87	810.02	8.0	0.745	B, C
7	1975.41 1975.11	5062.250 5063.017	6.234E-6 1.141E-4	2904.43 1960.21	944.22	5.9	0.767	B, C
8	1967.46 1967.32	5082.697 5083.058	5.504E-6 1.611E-4	2690.59 1843.03	847.56	3.7	0.361	B
9	1852.38 1852.06	5398.473 5399.396	3.041E-4 1.531E-6	1908.02 3032.69	1124.67	6.3	0.923	A, C
10	1764.78 1764.57	5666.434 5667.119	7.866E-7 9.486E-6	3211.21 2321.81	889.40	1.2	0.685	D
11	1764.78 1764.51	5666.434 5667.305	7.866E-7 2.843E-5	3211.21 2321.91	889.30	3.4	0.871	D
12	1764.57 1764.45	5667.119 5667.489	9.486E-6 2.731E-7	2321.81 3211.06	889.25	1.5	0.370	D

The fiber optic output laser and detector are integrated into a motorized mount housed inside of separate boxes. The transmit module is fiber optically coupled to a collimation lens followed by a refractive lens to filter combustion particles with similar absorption features as described above. The receiver module also contains a collimation lens and refractive lens before reaching the detector. This is designed to be insensitive to beam steering through the rocket plume. The equipment was designed to mitigate beam steering due to shock structures associated with up to a 4 meter rocket plume which could cause beam deflection up to 60mm.

3.3 Testbed and Data Acquisition System/Instrumentation

The testbed was built to use a variety of inlet gases. For the purposes of this thesis due to best results, air was chosen as the operating medium. The tube is resistively heated to warm the air to maintain operating conditions using a high amperage electrical power source. Directly

upstream of the heater, a water reservoir is resistively heated into steam and injected into the air flow as water vapor. At the end of the resistively heated chamber the mixture flows through the quartz pipe where the flow behavior is observed non-intrusively before exiting the nozzle. The testbed is instrumented with thermocouples and pressure transducers as shown in Figure 3. All the instrumentation equipment is recorded on a separate PC based data acquisition system that was calibrated for this unique experiment to compare TDLAS results.

Figure 4 shows the super heated water vapor injector. Figures 5-7 show the initial configuration of the TDLAS system. Figure 8 shows the observation test section. Figures 9 and 10 show the instrumentation of the data acquisition system and the TDLAS system, respectively. Figures 11-16 show pictorial views of the experimental setup. Further pictures, models and drawings for the experimental setup can be found in Appendices B-D.

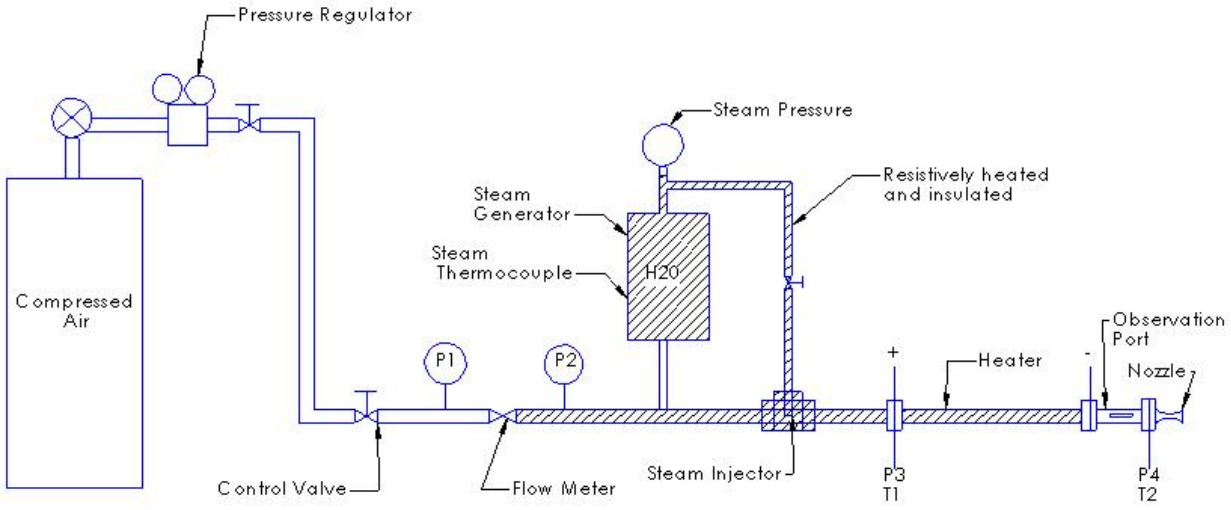

Figure 3 - Flow Diagram

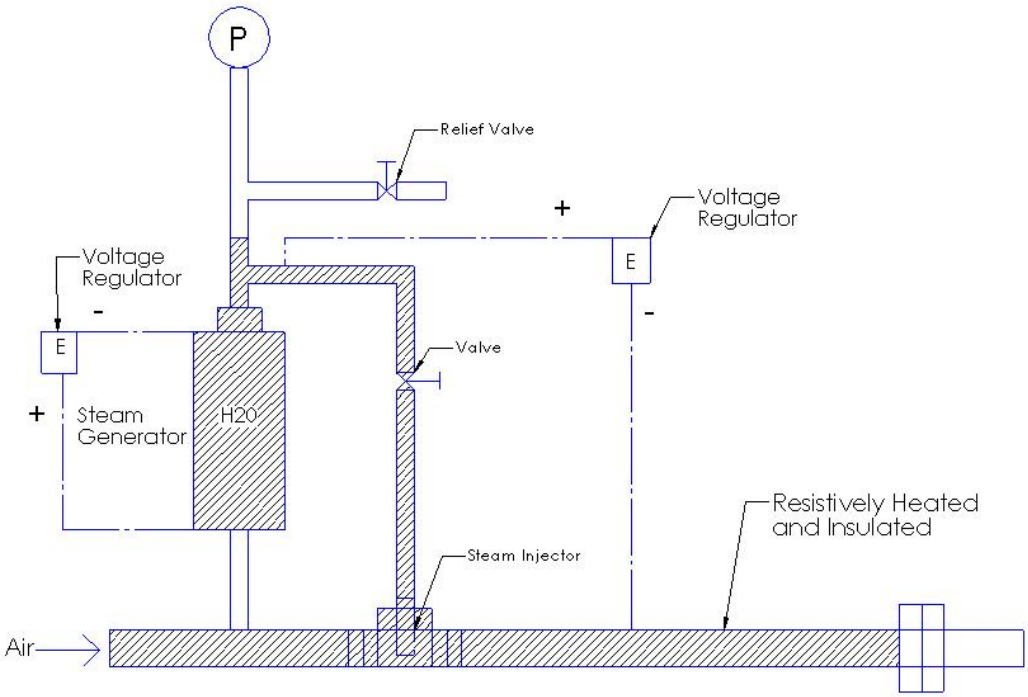

Figure 4 - Super Heated Steam Generator

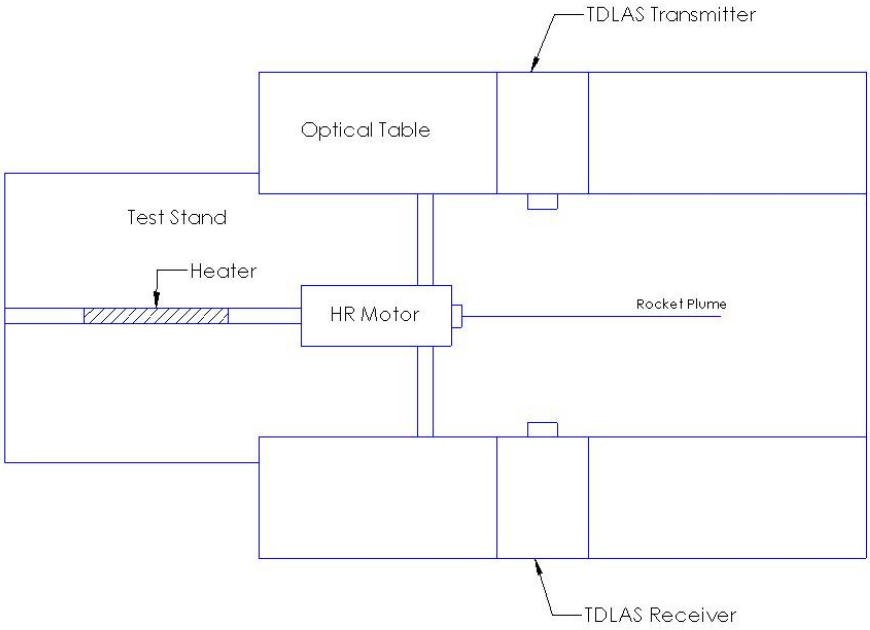

Figure 5 - Test Stand (Top View)

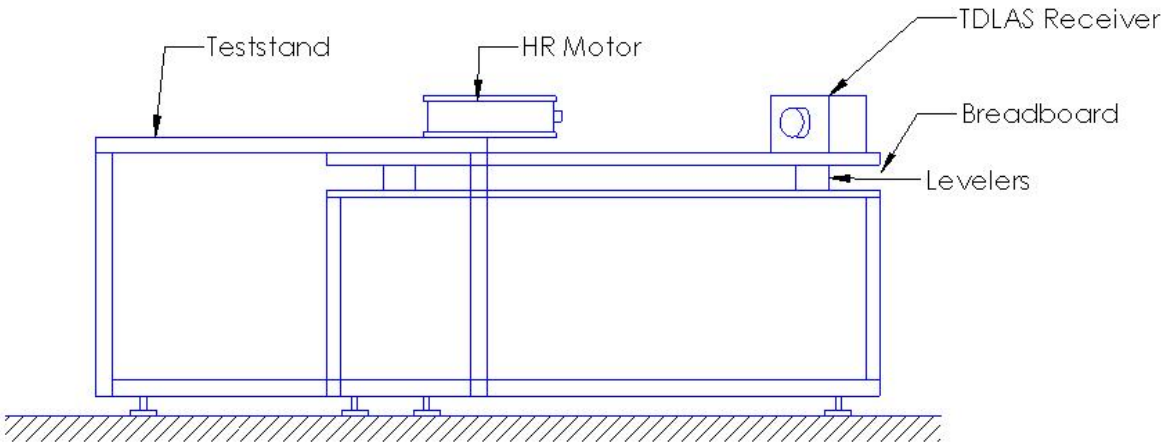

Figure 6 - Test Stand (Side View)

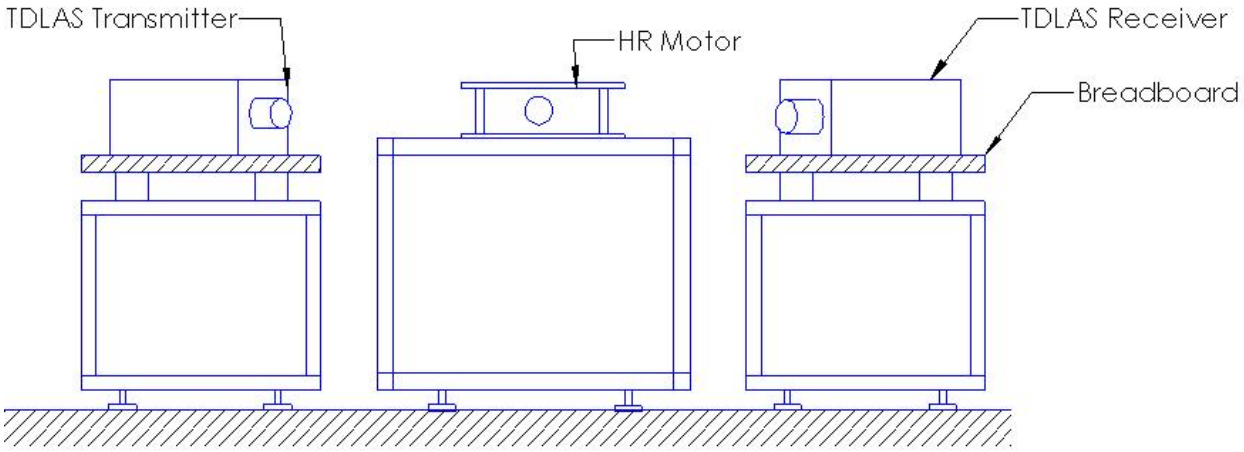

Figure 7 - Test Stand (Front View)

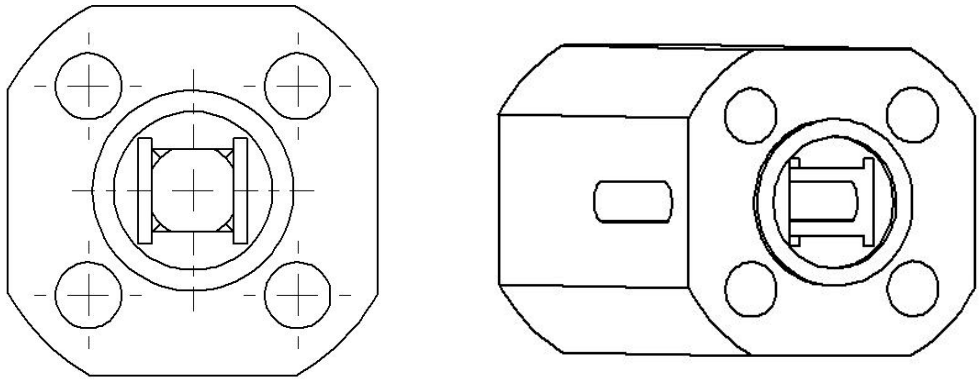

Figure 8- Quartz Containment (Observation Test Section)

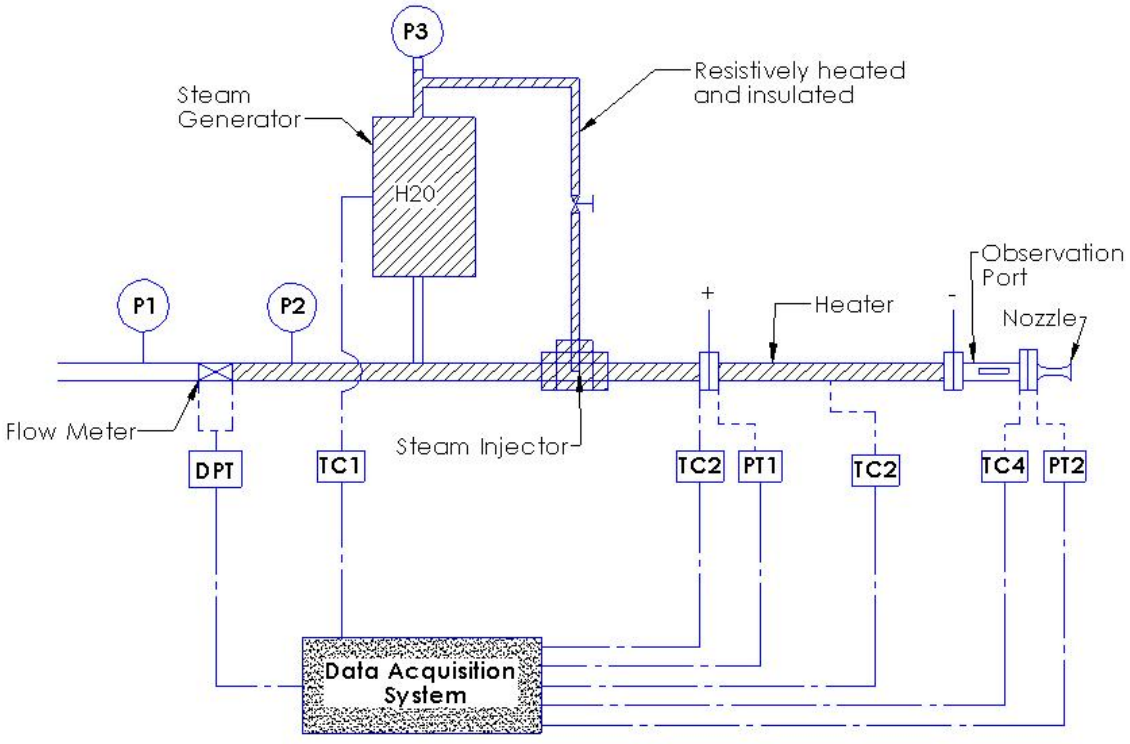

Figure 9 - Data Acquisition System Instrumentation Diagram

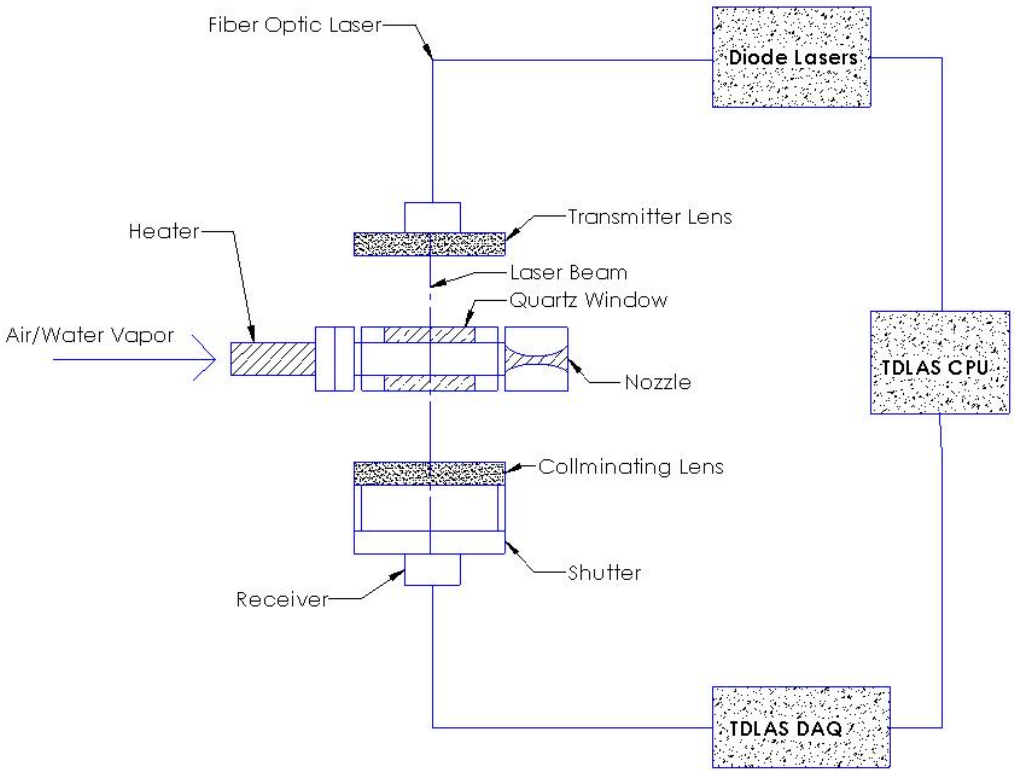

Figure 10 – Tunable Diode Laser Absorption Spectrometer Instrumentation Diagram

Figure 11- Pictorial View of Test Stand

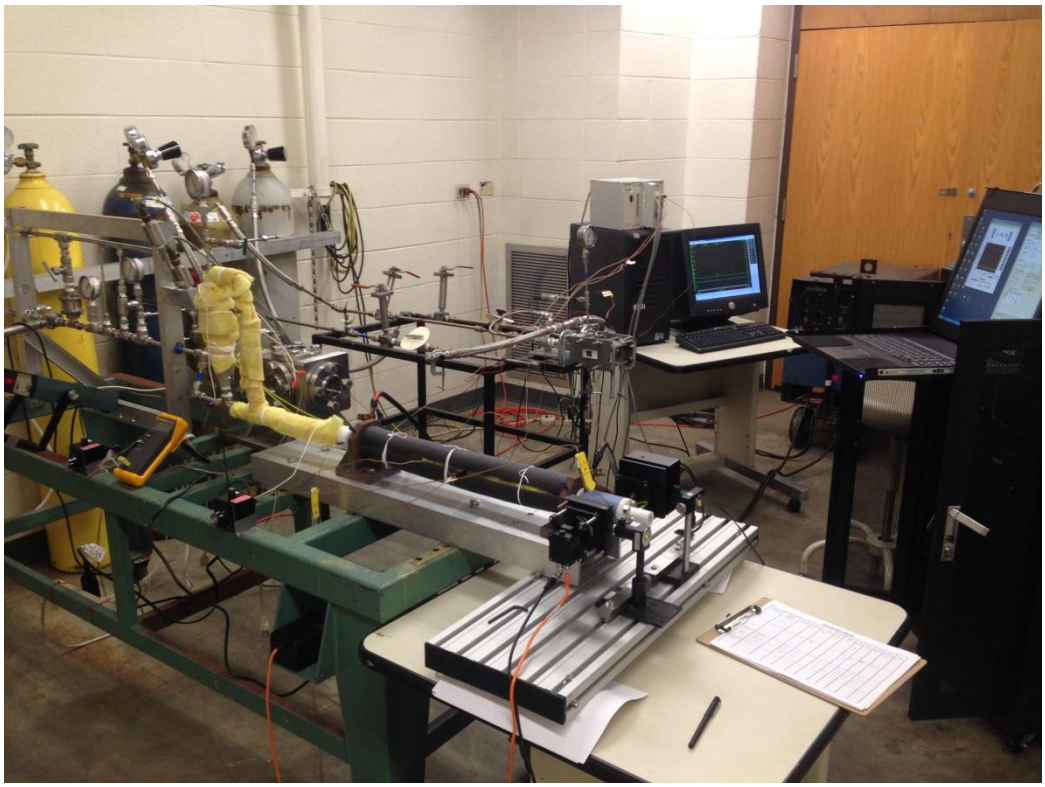

Figure 12- Experimental Layout showing Placement of Laser, Rocket, and DAQ

Figure 13- Experimental Layout showing Placement of Laser, Rocket, and DAQ

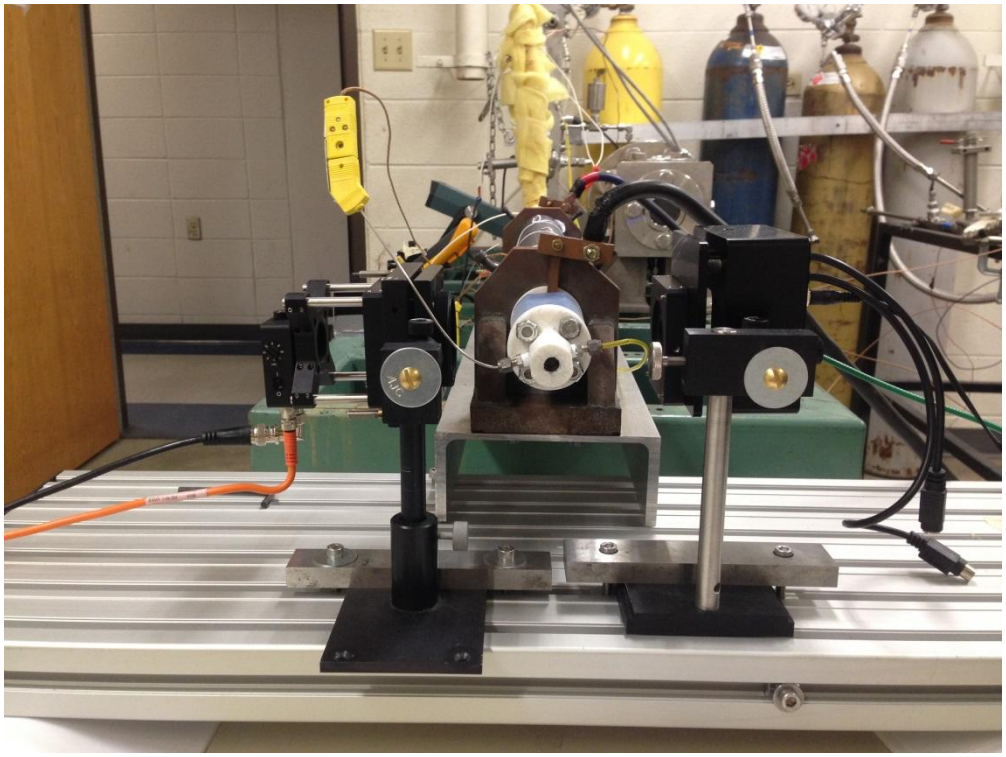

Figure 14- Experimental Layout showing Placement of Laser, Rocket, and DAQ

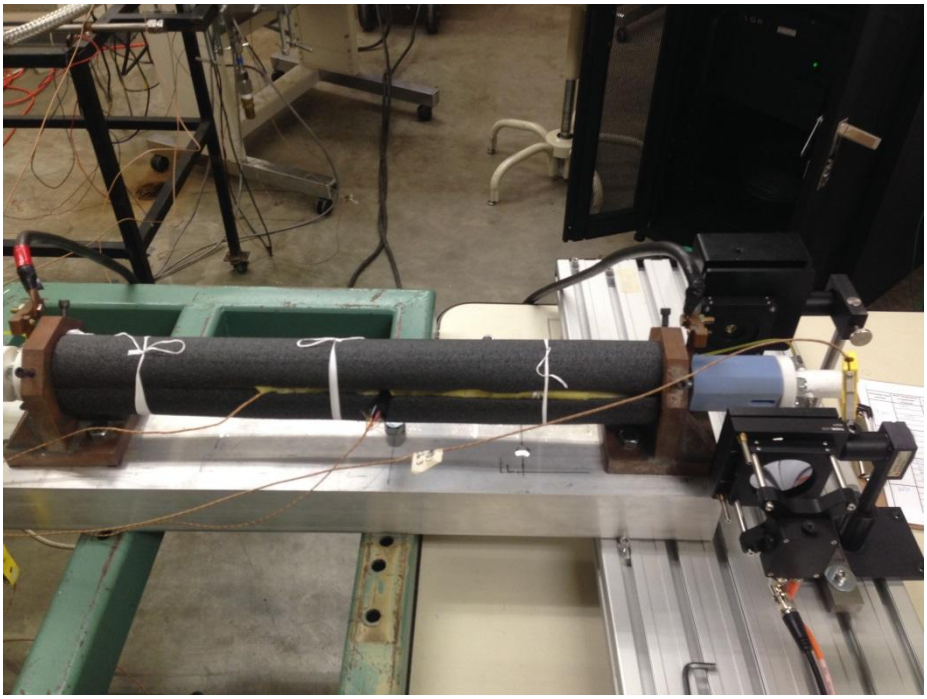

Figure 15- Experimental Layout showing Placement of Laser, Rocket, and DAQ

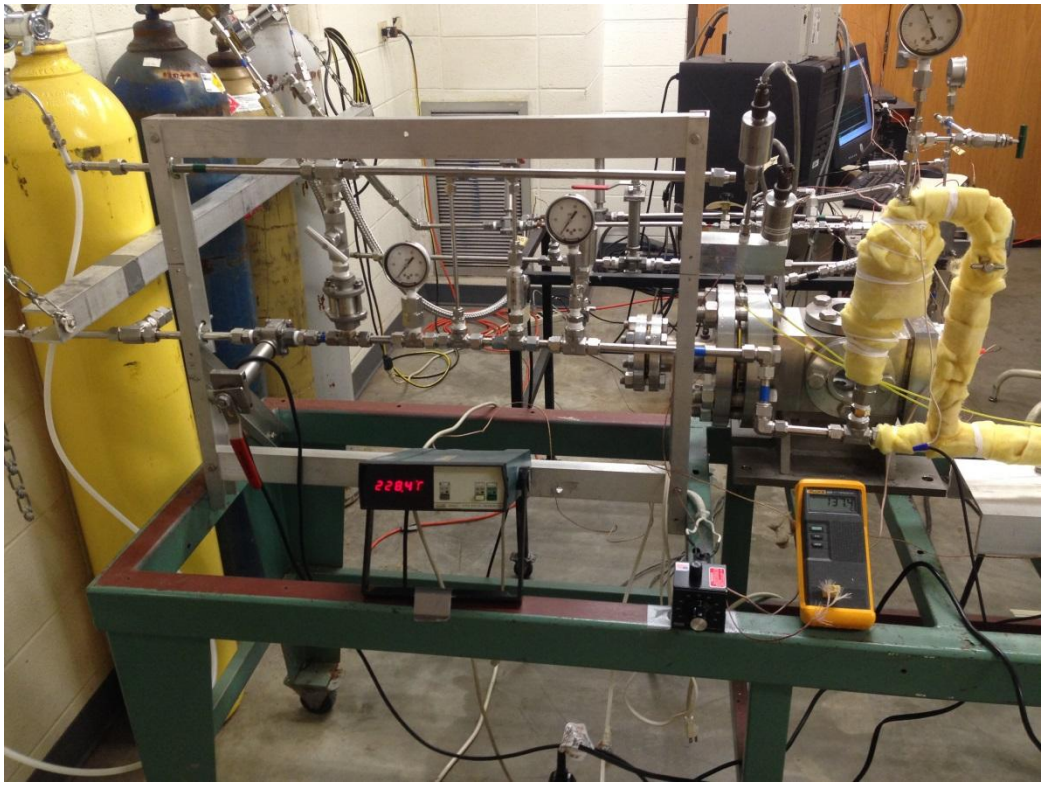

Figure 16- Experimental Layout showing Placement of Laser, Rocket, and DAQ

Chapter 4

Experimental Procedures

In order to capture accurate readings from the TDLAS, it must be verified that the laser and receiver are aligned optimally. The procedure for optical alignment is described in section 4.1 TDLAS Settings. In section 4.2 the operating conditions for the hybrid rocket motor simulator are monitored with the intrusive measurement devices.

4.1 TDLAS Settings

There are two programs that operate this gas analyzer. The programs allow the user to adjust input and output settings and write the receiver signals into the hardware from the DAQ system. The second program uses the relations described above to analyze and produce results for temperature, velocity, and concentration. The TDLAS uses 2 channels of 4 distributed feedback diode lasers and multiplexes each channel into 2 fiber optic cables capable of transmitting the frequency of the lasers. The settings on this equipment is set to observe spectral absorption lines of water vapor at 1343nM, 1388nM, 1392nM, and 1469nM. The lasers operate at frequency of 2MHz per channel.

The second program takes the recorded data which is measured in mV from the detector and uses a multi-peak Voigt fitting algorithm to return the integrated area under each transition for each data set per time. These results are then used to calculate the temperature and concentration of species as described above. For longer runs, data averaging is available to expedite computational time.

4.2 Operating Conditions

The rocket testbed has a multitude of flow variations to allow for a thorough parametric study. The main flow medium consists of bottled air and set to pressurize the system between 0-2 atm. The mass flow rate of the main line was calculated using pressure calibration correlations in Appendix E and equations found in Appendix F. Once the system is pressurized, the steam generator is resistively heated up to a desired constant temperature and injected into the main flow, which is then turned on. The pressure regulator in the air cylinder is then adjusted to achieve the desired velocity. The pipe upstream to the observation test section and nozzle is resistively heated to achieve a constant desired temperature. Once all parameters are constant and stable, the pre-aligned TDLAS is turned on to record the experiment. A parametric study is performed by holding the flow pressure constant and varying the temperature of the pipe and alternatively, holding the pipe temperature constant while varying the pressure source.

Chapter 5

Numerical Simulations

The heated section of the pipe upstream of the observation test section was modeled in 3D using a commercial CFD package (Fluent). The heat flux, inlet temperature, operating pressure, and mass flow rate are inputted into the 3D model to predict the flow behavior in the system. In Chapter 7 the results of the TDLAS measurements will be compared to the measurements of the thermocouples. The integrated average of the temperature profile will be the only condition compared to the TDLAS results. The axial distributions, profiles, and contour plots of these cases will be given in Appendix A.

5.1 CFD Mathematical Model

The goal of the numerical study was to provide additional simulations for comparison and calibration of the TDLAS. The physical model is the resistively heated test section leading to the observation port. The stainless steel pipe was given a constant heat flux along the length of the pipe corresponding to the operating conditions in the experimental setup. The boundary condition for the inlet of the pipe is the mass flow rate that was calculated from the data acquisition system in the experimental setup. The temperature upstream was given from the observed temperature read by the thermocouple. The outlet boundary condition assumes the pressure to be zero because the end of the pipe is open to the atmosphere.

A mesh independence study was performed to determine the consistency of the mesh cell sizes. The final mesh size is shown in figures 17-18. The following table shows the grid sizes and number of layers in the radial direction for the mesh independence study compared to the

exit velocity. The final mesh size was chosen for computational time and consistency with the higher mesh size cases and is shown in Table 2.

Table 2 – Matrix Showing Study to Determine Mesh Independence

	Maximum Cell Size	Axial Thickness (m)	Number of Cells	Inlet Pressure (psig)	Outlet Pressure (psig)	Inlet Velocity (m/s)	Number of Iterations	Exit Velocity (m/s)
Mesh 1	0.01	0.01	325422	151	0	1.05	237	1.52
Mesh 2	0.01	0.005	385423	1.51	0	1.05	325	1.53
Mesh 3	0.01	0.001	423014	1.51	0	1.05	414	1.55

The governing differential equations for this mathematical model use the Navier-Stokes equation, the energy equation, and the standard k-ε turbulence model equations. Fluent solves the following equations:

The continuity equation is given by:

$$\frac{1}{r}\frac{\partial}{\partial r}(rv) + \frac{\partial}{\partial z}(u) = 0 \tag{5}$$

The momentum equation in the r-direction is give by:

$$(V \cdot \nabla)v_r = -\frac{1}{\rho}\frac{\partial p}{\partial r} + g_r + v\left(\nabla^2 \mathrm{v_r} - \frac{\mathrm{v_r}}{\mathrm{r^2}}\right) \tag{6}$$

$$\text{Where: } \nabla^2 = \frac{1}{r}\frac{\partial}{\partial r}\left(r\frac{\partial}{\partial r}\right) + \frac{\partial^2}{z^2} \tag{7}$$

The momentum equation in the z-direction is give by:

$$(V \cdot \nabla)v_z = -\frac{1}{\rho}\frac{\partial p}{\partial z} + g_z + \nu(\nabla^2 v_z) \tag{8}$$

The energy equation is given by:

$$\rho c_p\left[\frac{\partial}{\partial t} + (V \cdot \nabla)T\right] = k\nabla^2 T + \mu[2(\in_{rr}^2 + \in_{zz}^2) + \in_{rz}^2] \tag{9}$$

$$\text{Where: } \in_{rr} = \frac{\partial v_r}{\partial r},\ \in_{zz} = \frac{\partial z}{\partial z},\ \in_{rz} = \frac{\partial v_r}{\partial z} + \frac{\partial v_z}{\partial r} \tag{10}$$

The equation of state is:

$$P = \rho RT \tag{11}$$

The previous equations are for a Newtonian fluid, steady-state, cylindrical, 3-dimensions, axisymmetric, and follow Stokes' assumptions.

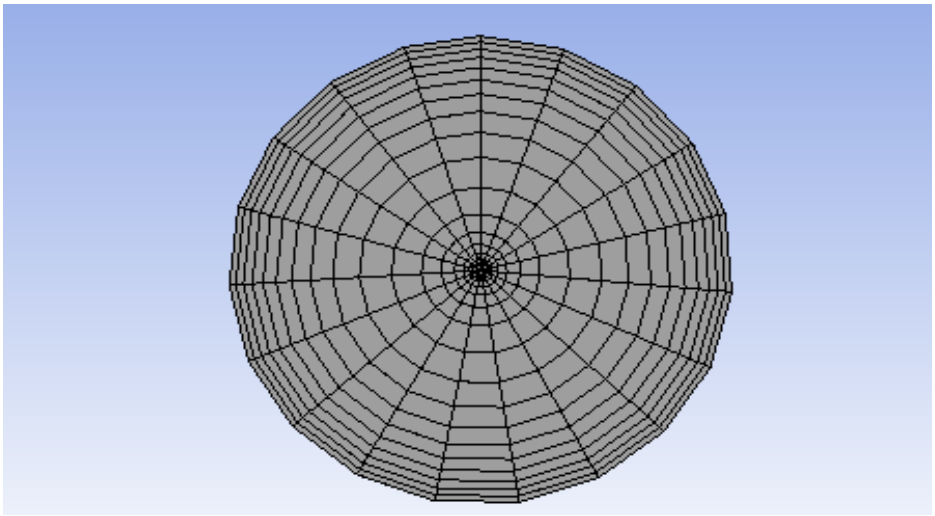

Figure 17- Cross Sectional Mesh

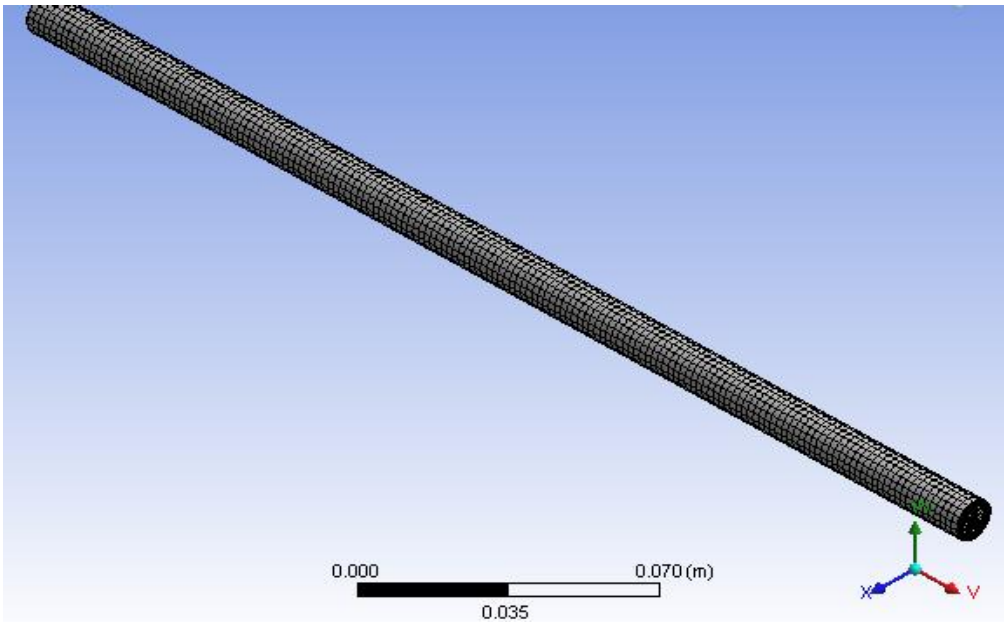

Figure 18- Isometric View of Mesh

5.2 CFD Settings

The following settings were used throughout the numerical simulations. Best results were found using pressure corrected method as opposed to the mass flow rate method. Convergence was improved by using 2nd order upwind discretization schemes for the momentum, energy, and k-epsilon equations.

Table 3 – Numerical settings of commercial package (Fluent)

Residuals	1.00E-06
Solution Method	Coupled
Numerical Method	Pressure Corrected
Discretization Scheme	2nd order upwind
Turbulent Model	K-epsilon
Energy Equation	On
Viscous Heating	On
Fluid	Air

To assure a fully developed flow in a relatively short pipe with a low mach number, the flow velocity was increased incrementally. The velocity was started uniform at a lower velocity and allowed to develop to the exit. The exit flow properties were then saved and inputted back into the inlet and the computational model was run again at the targeted velocities. This technique allows the inlet flow to be fully developed at the operating conditions of the experimental data.

Chapter 6

Results

There are 3 cases shown with increasing improvement in TDLAS measurements in sections 6.1-6.3. Section 6.1 shows the initial poor responses with the unaltered system and no super-heated steam injector. Sections 6.2 and 6.3 demonstrate the TDLAS response to the super-heated steam injector. Section 6.4 shows the requirements of water vapor concentration and the procedure required to obtain that concentration. Section 6.5 summarizes all modifications made to the testbed and measurement system to ensure better results. Section 6.6.1 shows the TDLAS results and operating conditions for 3 chosen cases of increasing temperature. Section 6.6.2 shows the numerical results for 1 of these cases. Finally, section 6.7 compares the results between the TDLAS and thermocouples.

6.1 Experiment 1 Run 1

The following table shows the experimental run sheet for the data that was recorded for each experiment. The operating conditions shown were recorded using the CP based DAQ system at the start of each run.

Table 4- Experimental Matrix Showing Operating Pressure, Mass Flow Rate, and Thermocouple Temperatures

Experiment	Parameter held constant	Wall Temperature or Upstream Pressure	Mass flow rate (lbm/s)	Run Number	Temp. Upstream (C)	Temp. Downtstream (C)	Duration (s)	Attenuation (dB)	File name	Steam Temp. (C)	Steam Pressure (psig)	Steam Valve Restriction
1	Wall Temperature 138 C	4 psi	0.0002	1	98	211	30	10	1	143	50 psi	30%
				2	101	220	33	10	2	144	50 psi	30%
				3	105	215	30	10	3	144	50 psi	60%
				4	103	212	32	10	4	144	50 psi	100%
				5	102	216	31	10	5	155	82 psi	60%

The results of Experiment 1 Run 1 are presented in the following figures. TDLAS settings were kept consistent and a time-averaged method was used to decrease post-processing time. This allows the two million sample readings per second to be time averaged by 100, which reduces the readings rate down to 20,000 measurements per second.

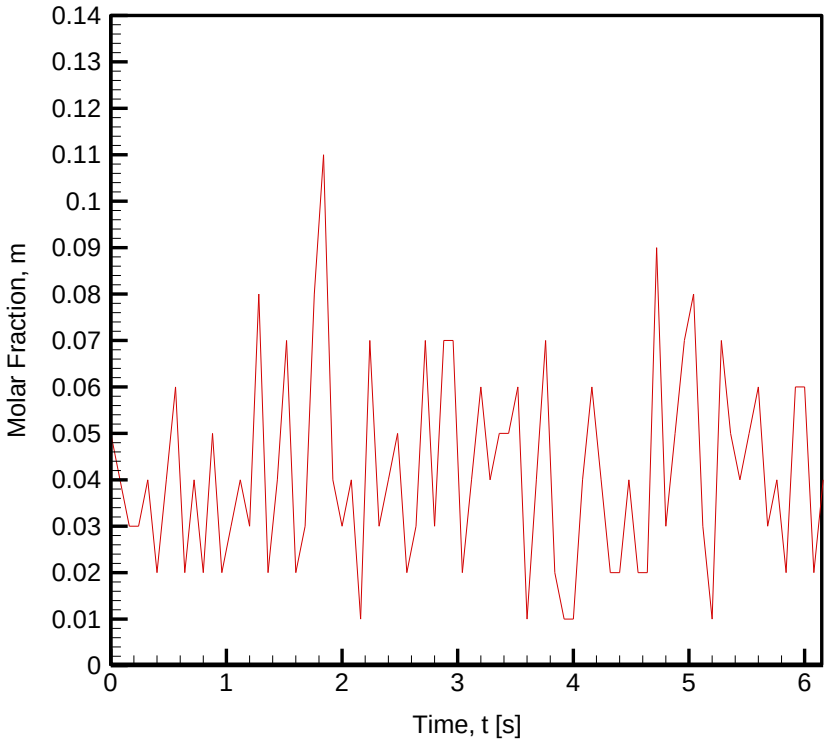

Figure 19- Experiment 1, Run 1: Water Vapor Molar Fraction v. time (TDLAS)

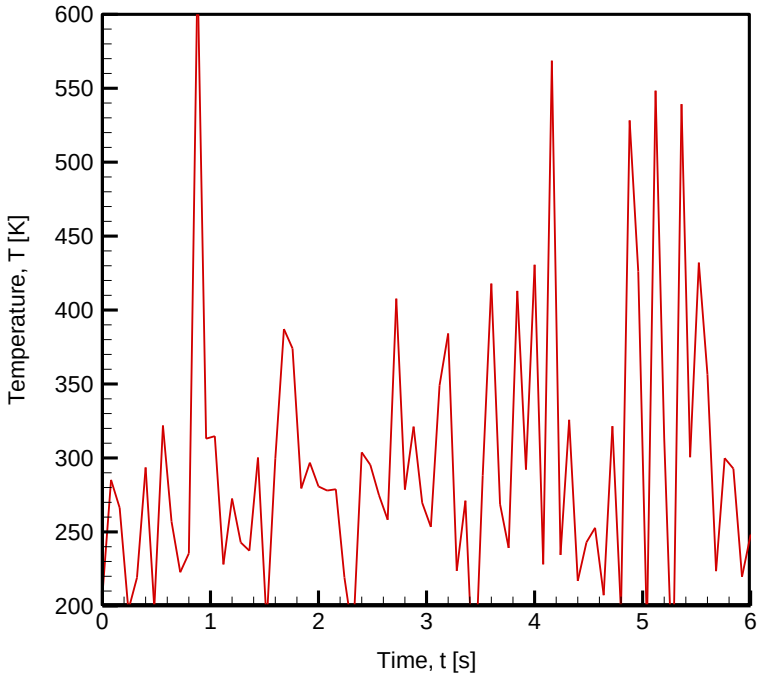

Figure 20- Experiment 1, Run 1: Temperature v. time (TDLAS)

The results in this experiment showed a small response to the introduction of steam into the system. However, the corresponding temperature is random and chaotic. This is mostly likely due to the low presence of water vapor molecules that the laser is observing. When the laser does not see enough molecules to observe, the change in intensity is so negligible that the smallest amount of ambient noise will overwhelm the system. There is a minimum concentration of water vapor for the TDLAS to make accurate readings. The design and implementation of the super-heated water vapor injector is for in the increase of water vapor concentration to meet this minimum requirement.

6.2 Experiment 2 – Run 3

In this experiment, the steam generator was heated to achieve superheated steam at 80 psi. This increase in differential pressure causes an increase in flow and thus concentration of steam into the system. The results for some of these experiments are shown below. The operating conditions are shown below as well.

Table 5 – Experiment 2 Operating Conditions

Experiment	Parameter held constant	Wall Temperature or Upstream Pressure	Mass flow rate (lbm/s)	Run Number	Temp. Upstream (C)	Temp. Downtstream (C)	Duration (s)	Attenuation (dB)	File name	Steam Temp. (C)	Steam Pressure (psig)	Steam Valve Restriction
2	Wall Temperature 138 C	2 psi	0.0001	1	105	215	40	10	6	155	82	100%
				2	107	220	45	10	7	168	86	100%
				3	103	217	51	10	8	168	82	100%
				4	100	216	55	10	9	180	80	100%
				5	105	211	45	10	10	180	84	100%
				6	107	214	56	10	11	175	80	100%
				7	110	215	60	10	12	179	82	100%

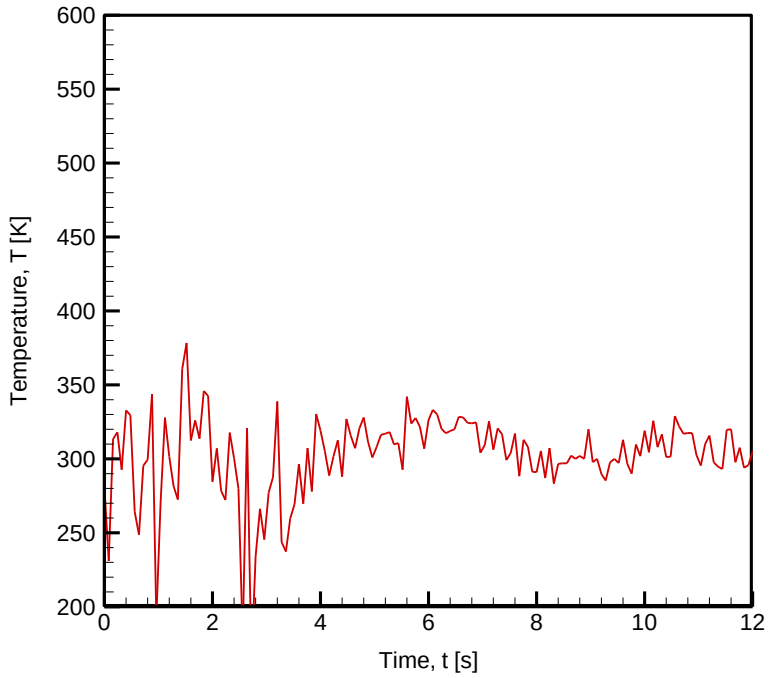

Figure 21- Experiment 2, Run 3: Temperature v. time (TDLAS)

The response to the steam is evident at 5 seconds when the steam valve was opened and steam was introduced into the system. Immediately the temperature consolidates as each laser sampling observes more steam particles and limits the signal to noise ratio. The super-heated water vapor pressure directly accounts for the concentration for water vapor in the system. Therefore, much experimentation was performed with the operating pressure of the injection system to optimize the amount of water vapor in the main flow line.

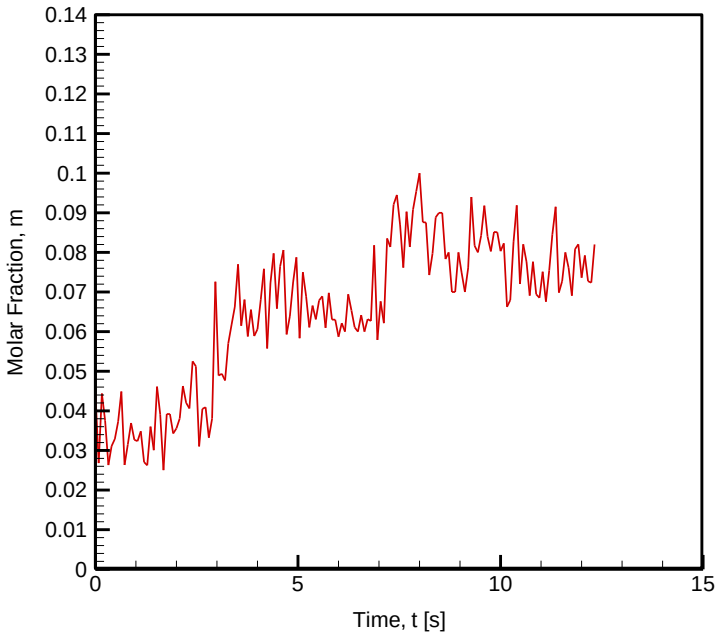

Figure 22- Experiment 2, Run 3: Water Vapor Molar Fraction v. time (TDLAS)

As with the plot of temperature, the introduction of steam is evident at 5 seconds. The molar fraction seems to smooth out between 8 and 12 seconds. This corresponds to an oscillating temperature around 37° Celsius. When comparing this to the tabulated thermocouple results for this experiment, the magnitudes are ± 1° C. This result achieved a valid response to the injected steam. However, the oscillations in concentration and temperature may be due to the periodic

absence of water vapor. Therefore, the steam generator was modified by increasing pressure to allow a higher density of steam to enter the system.

6.3 Experiment 2 – Run 6

Run 5 was repeated with the same operating conditions for a longer period of time to observe the oscillations over a longer period and are presented below. It can be seen that these oscillations continue over time and continue to hover around 37° Celsius. Again, the concentration of water vapor is speculated to be too low for an accurate reading.

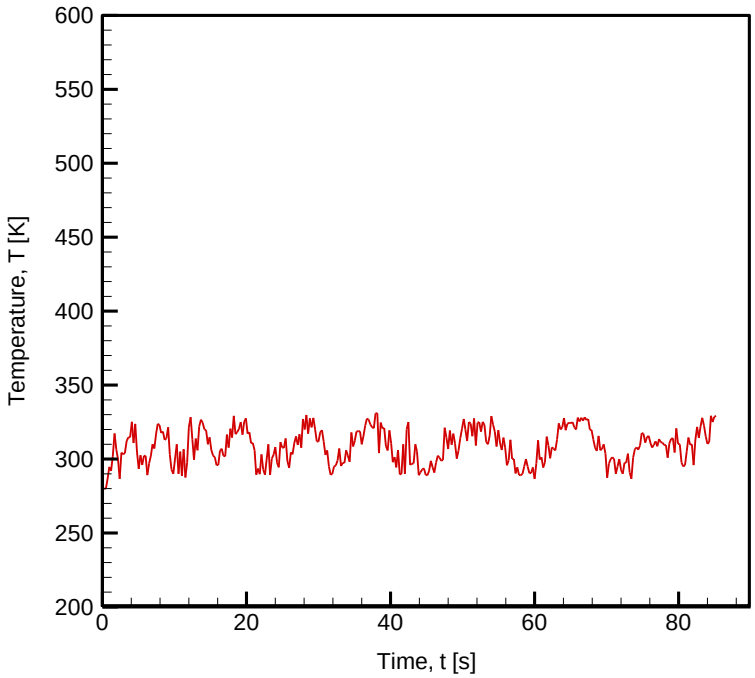

Figure 23- Experiment 2, Run 6: Temperature v. time (TDLAS)

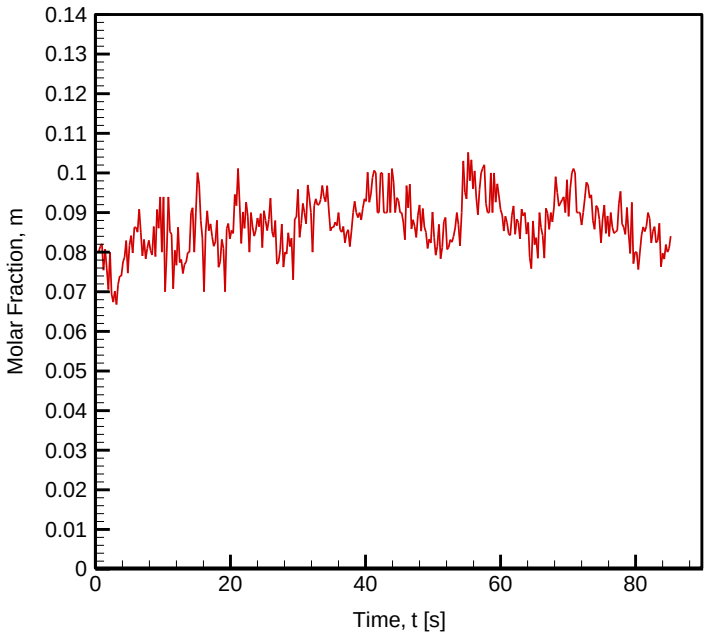

Figure 24- Experiment 2, Run 6: Water Vapor Molar Fraction v. time (TDLAS)

6.4 Selection Criteria for Results

The following figures show the TDLAS and DAQ system's respective response to the steam injector. A clear step function is visible in Figure 26. Based on these results, steady state conditions were measured between 5 and 30 seconds when the steam injector is turned on and off. Figure 27 shows the same response to the steam injection in the DAQ's recording of the thermocouples upstream and downstream of the heater. It can be seen from Figure 27, that the change in temperature is minimal, indicating the water vapor and air is at thermal equilibrium. The temperatures of the steam and the main air flow are at very similar magnitudes to ensure a homogenous mixture before the mixture reaches the heater.

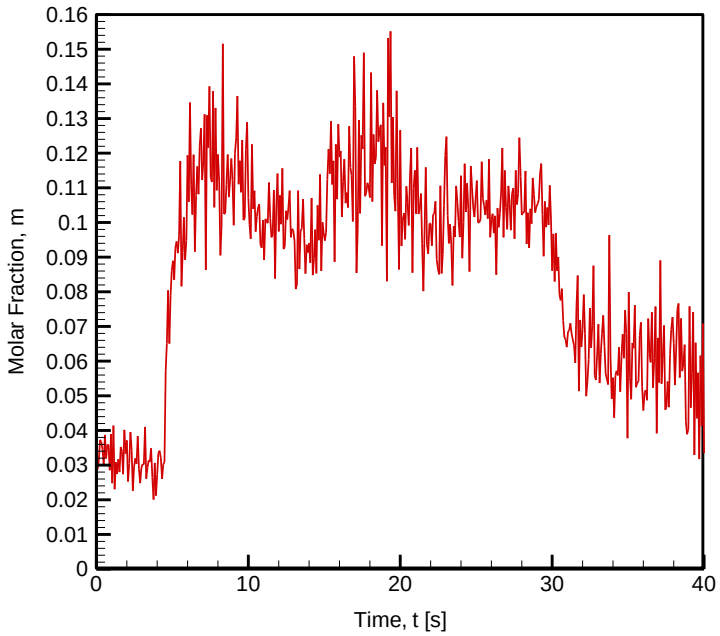

Figure 25– Experiment 2, Run 7: Molar Fraction Response to Steam Injector

Time, t [s]	Temperature, T [K]	Molar Fraction, m
0.00	284.0747	0.0293
0.08	304.7902	0.0288
0.16	312.0698	0.0313
0.24	312.5909	0.0373
0.32	345.8293	0.0368
0.40	340.7448	0.0345
0.48	351.9142	0.0302
0.56	277.8810	0.0387
0.64	327.9833	0.0319
0.72	335.8402	0.0360
0.80	339.3231	0.0358
0.88	284.0903	0.0285
0.96	291.2771	0.0390
1.04	240.7534	0.0248
1.12	288.9693	0.0414
1.20	208.1705	0.0230
1.28	281.7013	0.0308

Table 6 – Tabulated Data for Figure 26

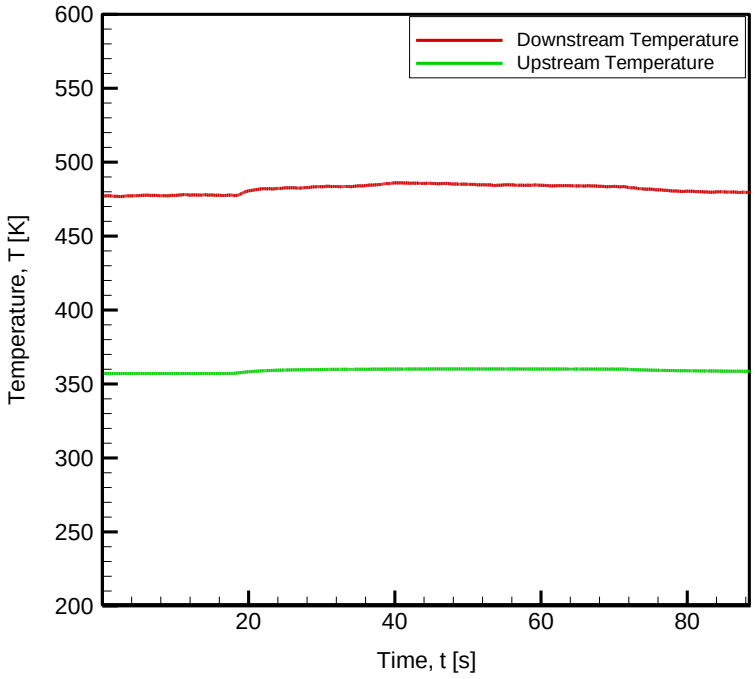

Figure 26- DAQ thermocouple results for Experiment 2, Run 7 showing response to Steam Injector

6.5 Modifications for Improvement

The equipment uses refracting lenses to filter out interference from combustion particles. The purpose of this application is to simulate combustion particles in a controlled and known manner for internal pipe flow. Therefore, alignment difficulties associated with these lenses was quickly theorized to limit the received intensity. The lenses were removed from the transmitter and receiver boxes and the experiments were performed again. While there was a measured increase in detected intensity, similarly chaotic results was recorded.

It was determined that the relatively weak signals were also due to the optical interference of the laser light passing through the quartz glass. The original quartz containment design used a round tube to maintain the integrity of the flow from the SS pipe to the observation

area. The quartz chosen has a 90% optical transmittance; however, due to the geometric curvature of the cylinder some of the photons are refracted and not observed by the detector. A secondary quartz containment was designed to use flat viewing windows so that this geometric interference could be corrected. The viewing area has a square profile but the hydraulic diameter was adjusted to maintain the same cross sectional area as to not disrupt the flow behavior.

Next, it was determined that poor results were due to optical alignment and possibly not meeting the minimum concentration of water vapor for an accurate reading. The transmitter and receiver were both removed from their kinematic mounts and integrated into an in-house optical table designed for this application. The transmitter and receiver were mounted to optical slides and fixed to the optical table. The boxes also limited the proximity the equipment could be placed to the testbed and thus increasing interference from ambient water vapor. This new setup drastically decreased the optical path length and the chance for ambient interference. Simultaneously, the steam generator was modified with additional power to increase the concentration of water vapor in the system.

6.6 TDLAS Results

Below, results of three cases are shown where the heat input is increased incrementally to observe the trend in the change in temperature. Figure 28 shows that the water vapor molar fractions for these cases are at a sufficient level (10% water vapor). The temperature will be shown for each case between the time ranges corresponding to steady state conditions. Finally the results will be compared with tabulated thermocouple results recorded with the CPU based DAQ system.

Table 7 –Operating Conditions for Final 3 Cases

Input Parameters	Experiment	Heater Power (kW)	Velocity (m/s)	Mass Flow Rate (lbm/s)	Mach Number	Reynolds Number	Wall Temp. (K)	Upstream of heater Temp. (K)
Operating Pressure: 2 psi Steam Restriction: Fully Open Steam Temperature: 140 C Steam Pressure: 46 psi	Exp. 2, Run 1	11	1.08	0.0002	0.19	4890	432	369
	Exp. 2, Run 5	24	1.32	0.0002	0.21	4296	684	373
	Exp. 2, Run 7	36	1.52	0.0002	0.22	3957	721	371

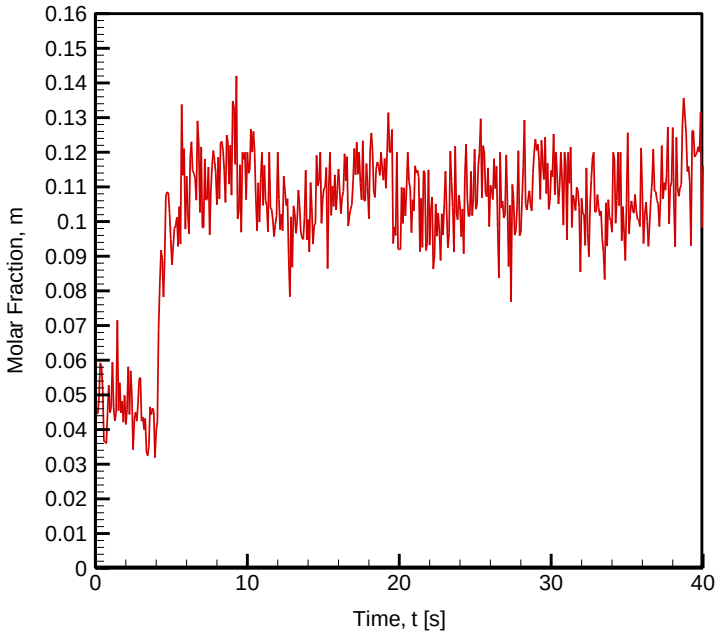

Figure 27- Experiment 3, Run 1: Water Vapor Molar Fraction v. time (TDLAS)

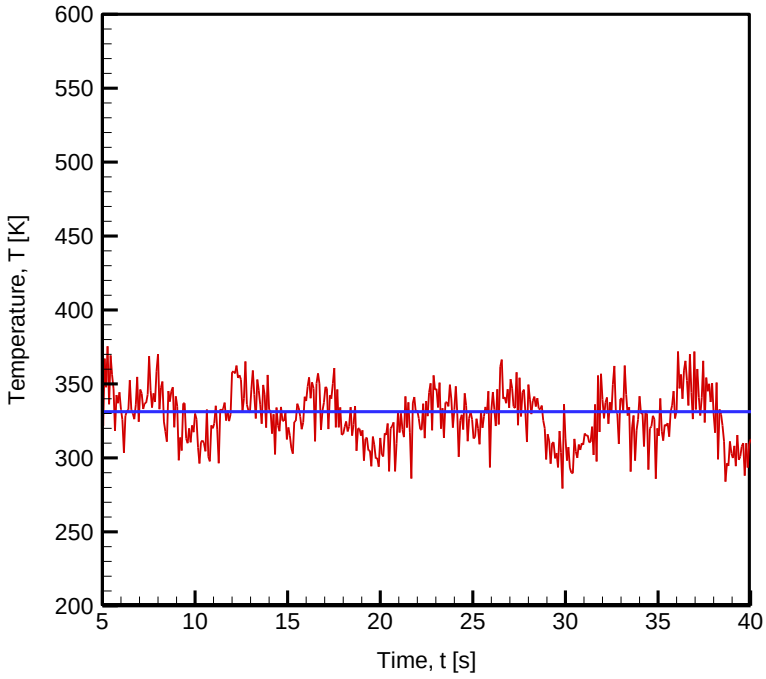

Figure 28- Experiment 3, Run 1: Temperature v. time (TDLAS)

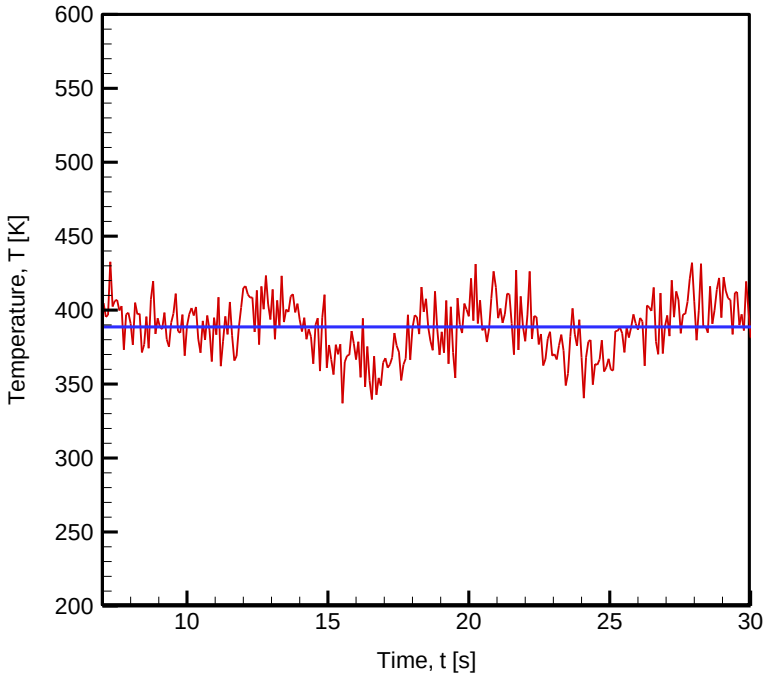

Figure 29- Experiment 2, Run 3: Temperature v. time (TDLAS)

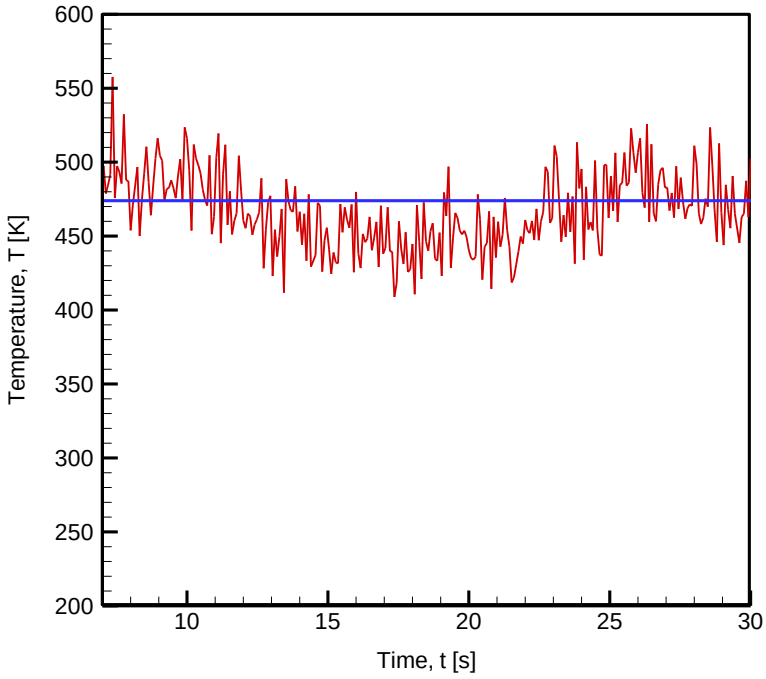

Figure 30- Experiment 2, Run 3: Temperature v. time (TDLAS)

It can be seen in the last 3 cases, the steady state temperature of the water vapor/air mixture was successfully observed to increase according to the heat flux prescribed to the heated section of the pipe. The water vapor concentration was successfully increased with the steam generator and injector system. The water vapor particles are essentially the seeded particles that are introduced into the system at the same temperature as the main flow to decrease mixing time and to achieve a homogenous flow. The molar fraction showed a strong correlation to the injected steam pressure as is predicted. As the pressure increases in the steam, the mass flow rate of water vapor into the main line increases.

6.7 Numerical Simulation of Exp. 2, Run 5

The following graphs show the predicted flow behavior of experiment 2, run 5. The results for the final 3 chosen cases are tabulated in Table 6. They will later be compared with the thermocouple data and the TDLAS results.

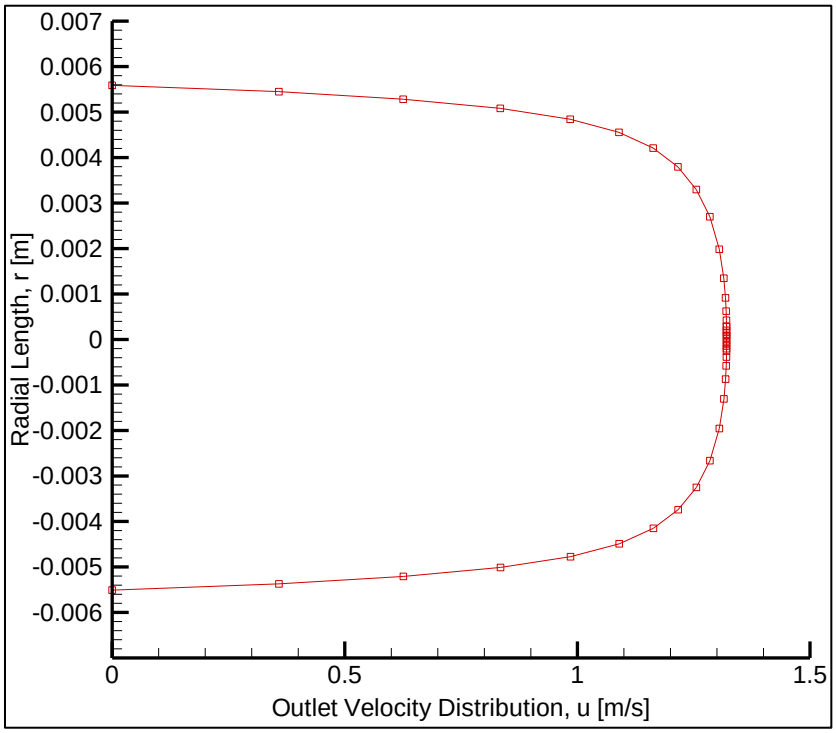

Figure 31- Fluent Velocity Distribution before Observation Port

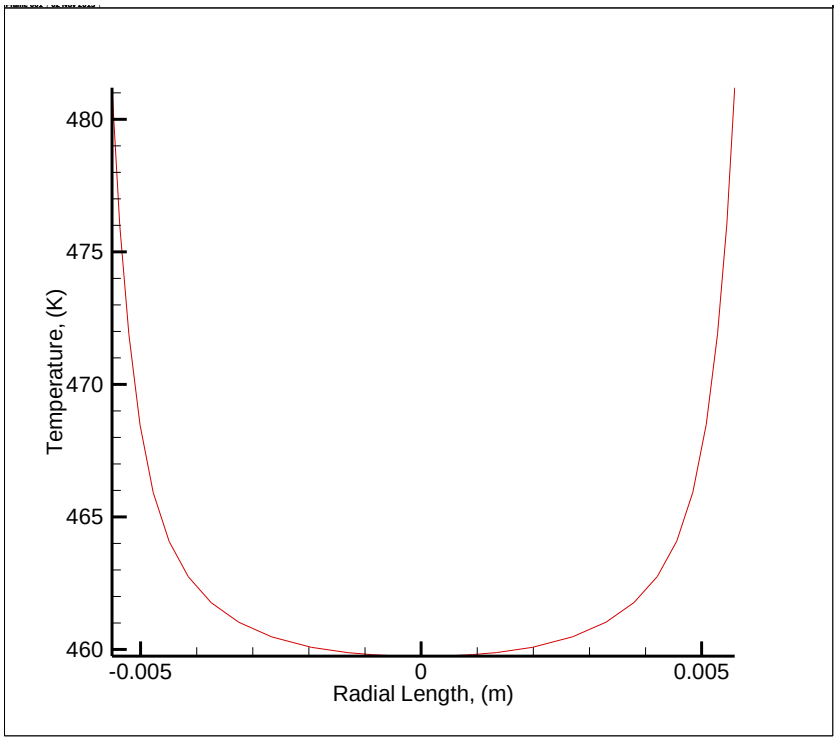

Figure 32– Fluent Temperature Distribution before Observation Port

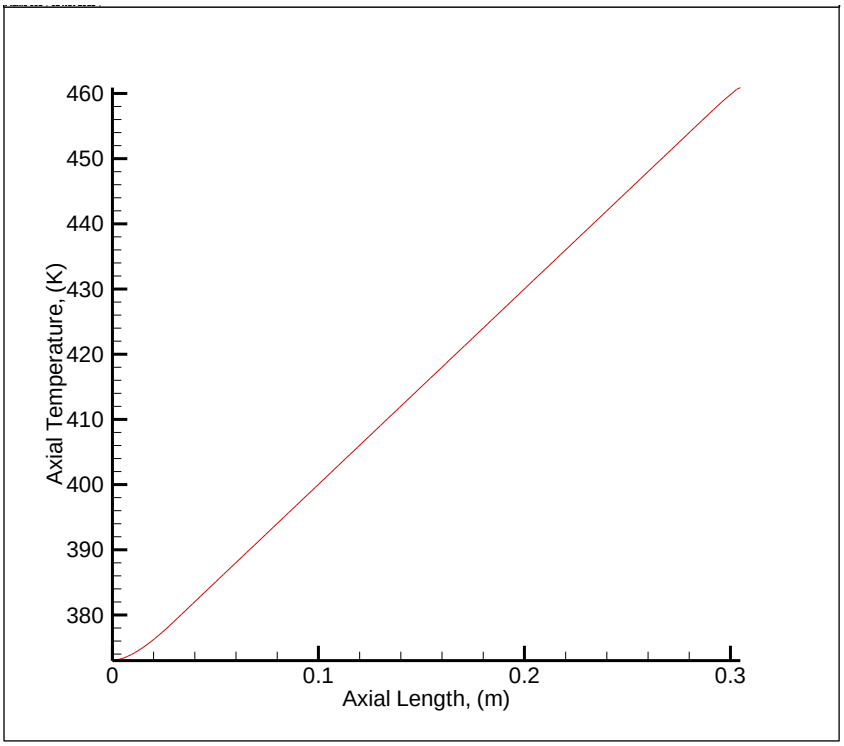

Figure 33– Fluent Axial Temperature Profile

Table 8 – Tabulated numerical results

Experiment 3 Simulations	Operating Pressure (psig)	Inlet Temperature (K)	Inlet Velocity (m/s)	Outlet Pressure (psig)	Heat Flux (kw/m2)	Predicted Averate Temperature at Outlet (K)
Run 1	1.05	370	1.08	0	11	385
Run 5	1.05	370	1.32	0	24	466
Run 7	1.05	370	1.52	0	36	532

The tabulated results show the predicted outlet average air temperature across the pipe for comparison with thermocouples and TDLAS results. Important flow characteristics are also show in Figures 32-34 for further information on the behavior of the flow.

6.8 Comparison of Results

The following table shows the final 3 cases with increasing heat inputs to the heater before the temperature is observed in the test article. The TDLAS results are compared to the thermocouples and the integrated average temperature profile predicted by the numerical study.

Table 9 –Results for Final 3 Chosen Cases

Experiment 3 Simulations	Operating Pressure (psig)	Inlet Temperature (K)	Inlet Velocity (m/s)	Outlet Pressure (psig)	Heat Flux (kw/m2)	Predicted Average Air Temperature at Outlet (K)
Run 1	1.05	370	1.08	0	11	385
Run 5	1.05	370	1.32	0	24	466
Run 7	1.05	370	1.52	0	36	532

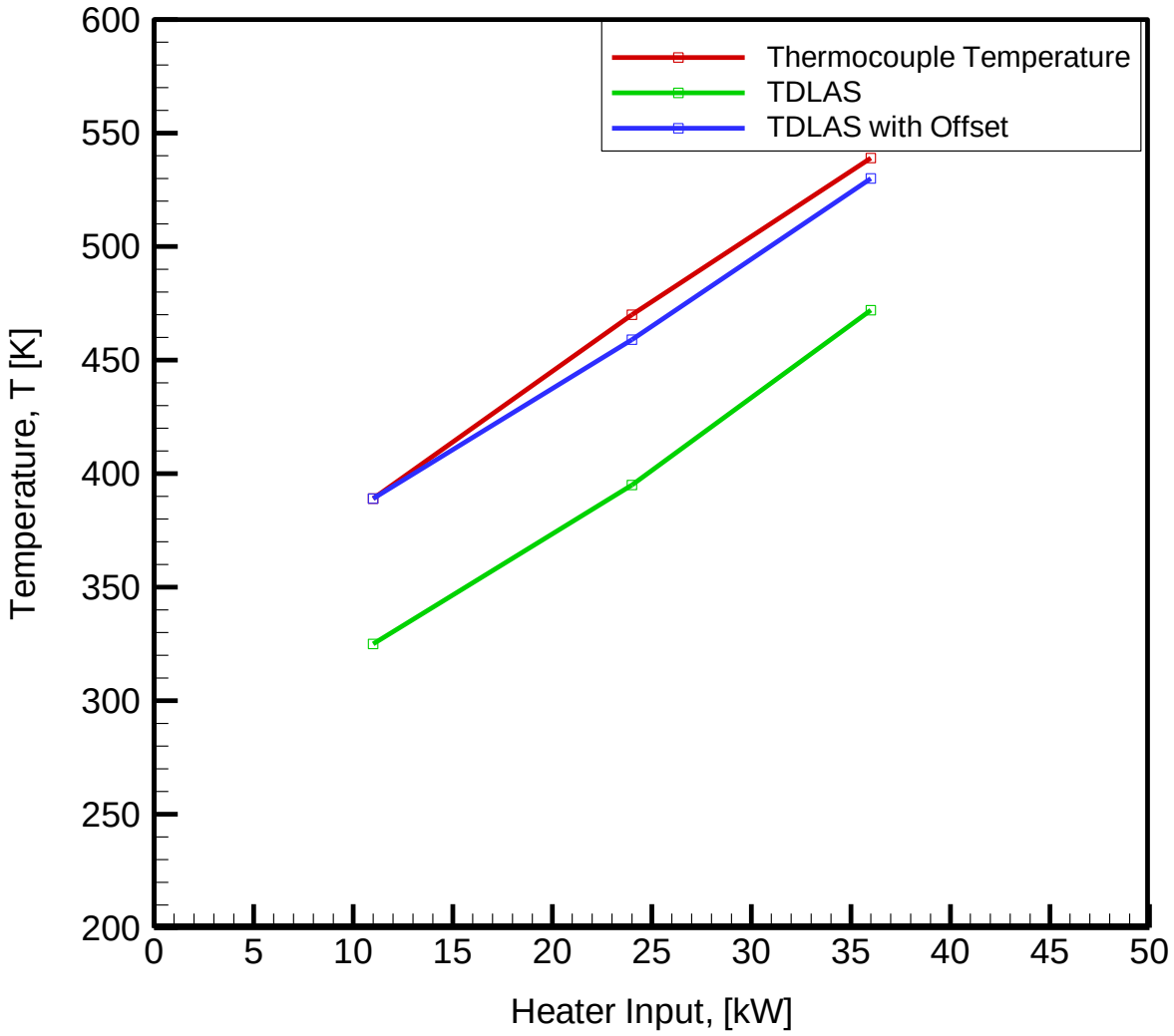

Figure 34 – Comparison of TDLAS and thermocouple temperatures for 3 chosen cases

6.9 Error Analysis

Great care was taken to ensure steady state conditions for the internal flow to be homogenous and constant temperature. There is some uncertainty associated with line-of-sight measurements due to the possibility of ambient water vapor in the path of the laser beam. As explained earlier, this was limited by the placement of the transmitter and receiver in close proximity to the test article. Due to the relatively low water vapor concentration in the UNO combustion lab, this interference is thought to be less than 5%.

In the experimental setup, there are errors associated with the thermocouples used as well as the pressure transducers used to calculate mass flow rate. Due to the imperfections associated with the insulation and calibration of the thermocouples, a ± 0.2 degrees C uncertainty is predicted. From the accuracy of the DAQ system and the pressure transducers used that enables a mass flow rate calculation, an uncertainty of ± 0.5% is assumed.

We are aware the measurement of flow temperature between the TDLAS and thermocouples in the center of flow are not measured at exactly the same place. But the relatively low flow rate and close proximity allows us to estimate an uncertainty of ± 5%.

Chapter 7

Conclusion

The goal of this study was to take a prototype tunable diode laser absorption spectrometer designed to measure high temperature water vapor combustion gases (rocket plume studies) and adapted for low temperature and low velocity internal flows.

Based on the present study, one can conclude that the TDLAS can be successfully adapted to measurement of low temperature internal gas flows. The present study results, for fluid temperature range of 300K-600K at velocities corresponding to 0.2 Mach number, indicate that the TDLAS measurements under estimate the gas temperature with a deviation of 20%. It is concluded that a calibration of the measurement system with an offset of 70K would be necessary to obtain accurate tunable diode laser absorption measurements. In order to properly calibrate the current TDLAS system, additional parametric studies would need to be performed.

Chapter 8

Recommendations

For improved results, it is recommended that the main flow line should be reduced in diameter. This reduction in pipe size would help improve the fluid's response to the resistive heater. The maximum attainable temperature would be increased substantially as the fluid would have more surface area per unit volume of contact with the pipe. Ideally, the fluid temperature would be heated to combustion temperatures to verify similar results with combustion flow. Once, validated then it would be feasible to parametrically define the limitations of this equipment in a well-controlled flow behavior.

To assure a homogenous mixture, it is recommended to resistively heat a large portion of the main line prior to steam injection. This will assure that the two flows are at the same temperature during mixing. The homogenous mixture will assure consistent measurements downstream at the observation port.

Additionally, error associated with line-of-sight measurements could be limited by blowing nitrogen outside of the test article. This will eliminate the ambient water vapor that could cause added noise to the system.

List of References

Allen, M.G, Furlong, E.R, et al., 2002, "*Tunable Diode Laser Sensing and Combustion Control*", Applied Combustion Diagnostics, Page No. 479-798, Taylor and Francis, NY.

Arroyo, M.P, Hanson, R.K, 1993, "*Absorption Measurements of water Vapor Concentration, Temperature and Line Shape Parameters Using a tunable In GaAsp Diode Laser*", Applied Optics, Vol. 32, Page No. 6104-6116.

Arroyo, M.P, Langlios, S, et al., 1994, "*Diode Laser Absorption Technique for Simultaneous Measurements of Multiple Gas dynamics Parameters in High Speed Flows Containing Water Vapor*", Applied Optics. 33, Page No. 3296-3307.

Baer, D.S, Hanson, R.K, et al., 1994, "*Multiplexed Diode Laser Sensor System for Simultaneous H_2O and O_2 and Temperature Measurements*", Optical Letters, Vol. 19, Page No. 1900-1902.

Baer, S.B. and Fahrland, A., 2009, "*High Sensitivity Diagnostics for Combustion*," JANNAF paper published in CPIAC JSC CD-60, Abstract No. 2009-0105CD

Brown, L.R, Plymate, C, 2000, "*Experimental Line Parameters of the Oxygen A Band at 760mm*", Journal of Mol. Spectroscopy 199, Page No. 166-179.

Cai, T., Gao, G., Gao, X. , Chen, W., and Liu, G., 2010, "Diode laser measurement of line strengths and air-broadening coefficients of CO_2 and CO in the 1.57 μm region for combustion diagnostics," Molecular Physics, Volume 108, Issue 5, Pages 539-545.

Chang, L.S., Jeffries, J.B., and Hanson, R.K., 2010, "Mass flux sensing via tunable diode laser absorption of water vapor," 48th AIAA Aerospace Sciences Meeting, Article number 2010-0303, Orlando, FL.

Chou, S.I., Baer, D.S., and Hanson, R.K., 1997, "*Diode-Laser Absorption Measurements of CH_3Cl and CH_4 near 1.65μm,"* Applied Optics, Vol. 36, No.15, pp. 3288-3293.

Choi, G.M, 2003, "*Combustion Control with Pressure Gradient and Development of DFB Diode Laser Sensor*", Annals of Optics, Volume 5, Geumjeong-gu, Busan 609-735, Republic of Korea.

Farooq, A., Jeffries, J.B., Hanson, R.K., 2009, *"Measurements of CO_2 concentration and temperature at high pressures using 1 f-normalized wavelength modulation spectroscopy with second harmonic detection near 2.7 μm."* Applied Optics, Volume 48, Issue 35, Pages 6740-6753.

Furlong, E.R, Baer, D.S, et al., 1998, "*Real time adaptive combustion Control using Diode Laser Absorption Sensors*", Proceedings of Combustion Institute, Vol 28, PP.108-111, Combustion Inst, Pittsburg, PA.

Furlong, E.R, Mihalcea, R.M, et al., 1999, "*Diode Laser Sensor for Real Time Control of Pulsed Combustion System*", AIAA Journal, Page No. 732-737.

Hanson, R.K, Jeffries, J.B, 2004, "*Sensors for Advanced Combustion Systems*", GCEP Technical Report.

Houle, A.J., Nakakita, K., Heltsley, W.N., Jeffries, J.B., Hanson, R.K., 2006, *"Diode laser absorption measurements of supersonic flow in an expansion tube."* AIAA/ASME/SAE/ASEE 42nd Joint Propulsion Conference, Sacramento, CA.

Li, H. , Farooq, A., Jeffries, J.B., and Hanson, R.K., 2007, *"Near-infrared diode laser absorption sensor for rapid measurements of temperature and water vapor in a shock tube."* Applied Physics B: Lasers and Optics, Volume 89, Issue 2-3, Pages 407-416.

Li, F., Yu, X.-L., Chen, L.-H., and Zhang, X.-Y., 2009, "*Temperature and water vapour concentration measurements of CH_4/Air premixed flat flame based on TDLAS*," Journal of Experiments in Fluid Mechanics ,Volume 23, Issue 2, Pages 40-44.

Liu, J.T, Rieker, G.B, et al., 2005, "*Near-Infrared Diode Laser Absorption Diagnostics for Temperature and Water Vapor in a Scramjet Combustor*", Applied Optics, Vol.32, Page No. 6701-6711.

Liu, J.T.C, Jeffries, J.B, et al., 2003, "*Diode Laser Absorption Diagnostics for Measurements in Practical Combustion Flow Fields*", 39th AIAA Joint Propulsion Conference.

Liu, J.T.C, Jeffries, J.B, et al., 2004, "*Wavelength Modulation Absorption Spectroscopy With 2F Detection Using Multiplexed Diode Lasers for Rapid Temperature Measurements in Gaseous Flow*", Applied Physics B, 78, Page No. 503-511.

Liu, X., Jeffries, J.B., and Hanson, R.K., 2007, " Measurement of nonuniform temperature distributions using line-of-sight absorption spectroscopy," AIAA Journal, Volume 45, Issue 2, February 2007, Pages 411-419.

Liu, X., Jeffries, J.B., Hanson, R.K., Hinckley, K.M., and Woodmansee, M.A., 2006, "Development of a tunable diode laser sensor for measurements of gas turbine exhaust temperature," Applied Physics B: Lasers and Optics, Volume 82, Issue 3, Pages 469-478.

Mihalcea, R.M, Bear, D.S, et al., 1997, "*Advanced Diode Laser Absorption Sensor for In-Situ Combustion Measurements of CO2, H2O, and Temperature*", Twenty-Seventh Symposium (International) on Combustion, the Combustion Institute, Pittsburgh.

Mihalcea, R.M, Bear, D.S, et al., 1997, "*Diode-Laser Sensor for Measurements of CO, CO2, CH4 in Combustion Flows*", Appl. Opt. 36, Page No.8745.

Mihalcea, R.M., Baer, D.S., and Hanson, R.K., 1998, "*A Diode-Laser Sensor System for Combustion Emission Measurements*," Meas. Sci. Technol., Vol.3, pp. 327-338.

Mihalcea, R.M., Baer, D.S., and Hanson, R.K., 1998, "*Advanced Diode-Laser Sensor for in situ Combustion Measurements of CO2, H2O, and gas Temperature,"* AIAA 36th Aerospace Science Meeting, paper no. AIAA-98-0237.

Paulsen, K.G. , Dang, D.D., 2011, *"Tunable diode laser spectroscopy for high temperature combustion,"* Proceedings of the Annual ISA Analysis Division Symposium, League City, TX.

Peterson, K.A, Daniel, B, 2000, "*Diode Laser-Based Tunable Ultraviolet Sources for Combustion Diagnostics*", Optical Society of America, LACEA 2000.

Rothman, L.S, Jacquemart, D, et al., 2005, "*The HITRAN Molecular Spectroscopic Database*", Journal of Quantitative Spectroscopy and Radioactive Transfer, Vol. 96, Page No. 130-204.

Sanders, S.T, Baldwin, J.A, et al., 2000, "*Diode Laser Sensor for Monitoring Multiple Combustion Parameters in Pulse Detonation Engines*", Proceedings of the Combustion Institute, Vol. 28, Page No. 587-594, Pittsburg, PA.

Sanders, S.T., Wang, J., Jeffries, J.B., Hanson, R.K., 2001, "*Diode-Lasers Absorption Sensor for Line-of-Sight Gas Temperature Distribution,"* Applied Optics, Vol. 40, pp 4405-4415.

Sanders, S.T, Mattison, D.W, et al., 2002, " *Sensors for High-Pressure, Harsh Combustion Environments using Wavelength-Agile Diode Lasers*", Proceedings of the Combustion Institute, Vol. 29, Issue 1, Page No. 2661-2667.

Vallon, R., Soutadé, J., Vérant, J.-L., Meyers, J., Paris, S., and Mohamed, A., 2010, "A compact tunable diode laser absorption spectrometer to monitor CO_2 at 2.7 μm wavelength in hypersonic flows," Sensors, Volume 10, Issue 6, Pages 6081-6091.

Veale, J.R., Wang, L.G., and Gallgher, T.F., 1992, "*Remote Sensing of O_2 in a Supersonic Combustor Using Diode-Lasers and Fiber-Optics,"* 4th International AIAA Aerospace Planes Conference, Orlando, Fl.

Zhou, X, Jeffries, J.B, et al., 2005, "*Development of Fast Temperature Sensor for Combustion Gases Using a Tunable Diode Laser*", Applied Physics, Vol. 81, Page No.711-722.

Zhou, X., Jeffries, J.B, et al., 2007, "*Wavelength Scanned Tunable Diode Laser Temperature Measurements in a Model Gas Turbine Combustor*", AIAA Journal Vol. 45, No. 2.

Appendix A

Results of Numerical Studies

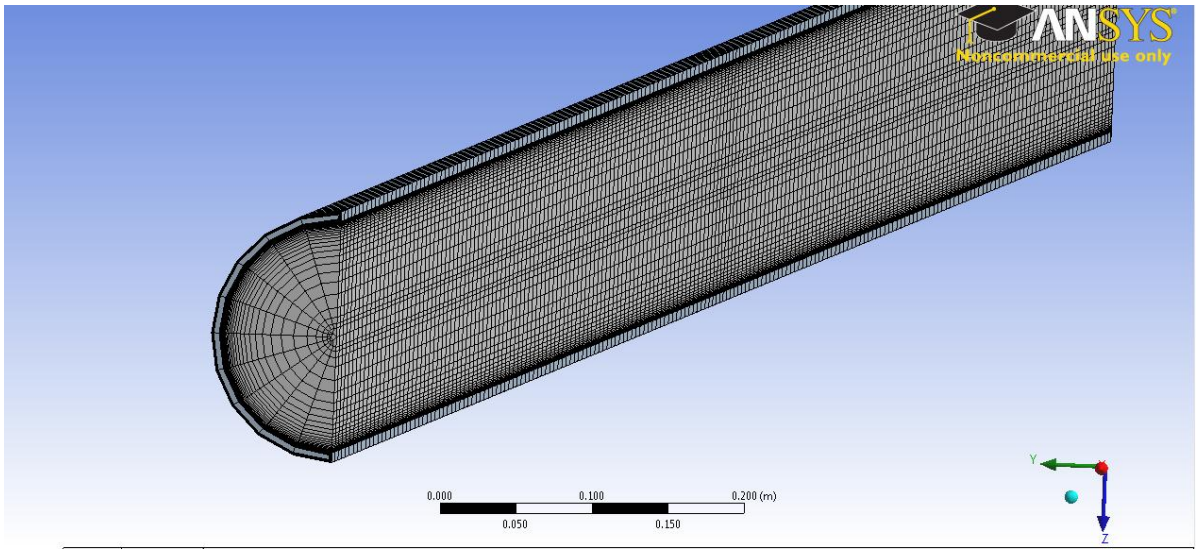

Figure A.1- Mesh for CFD Studies

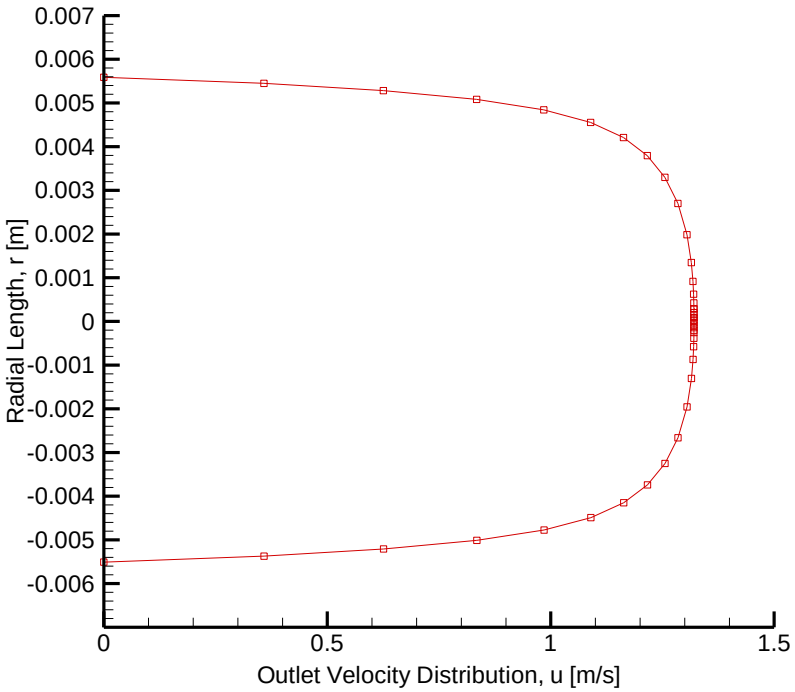

Figure A.2- Predicted velocity distribution at the exit

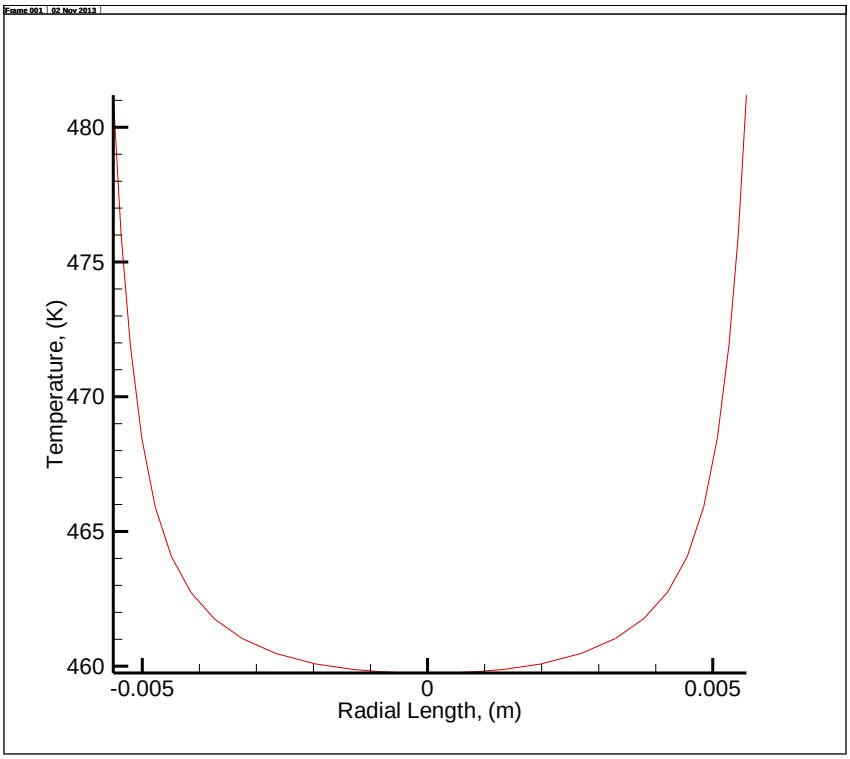

Figure A.3- Predicted temperature distribution at the exit

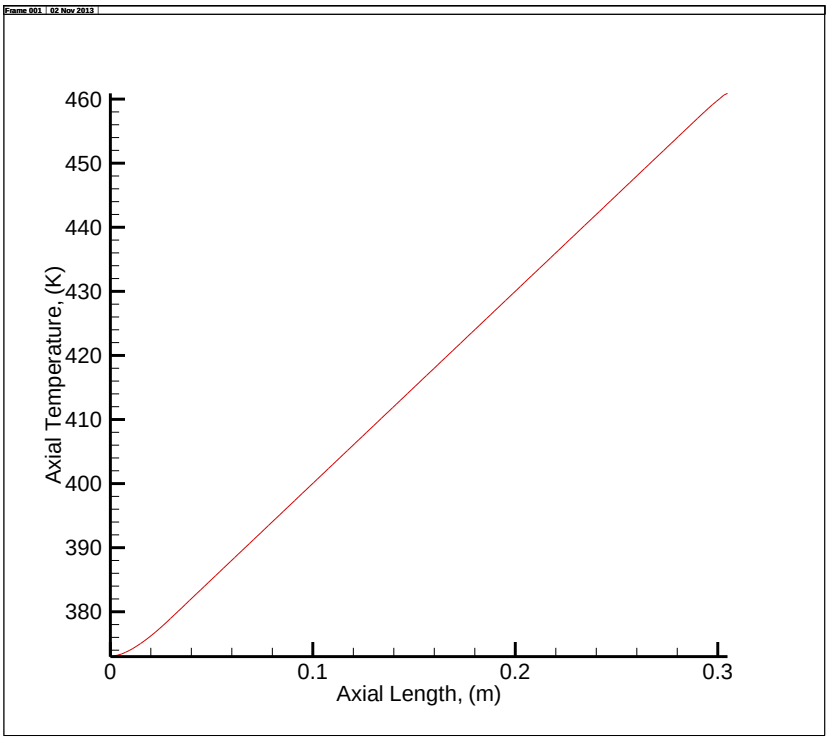

Figure A.4- Predicted axial temperature distribution in the pipe

Appendix B

Rocket Motor Simulator Pictures

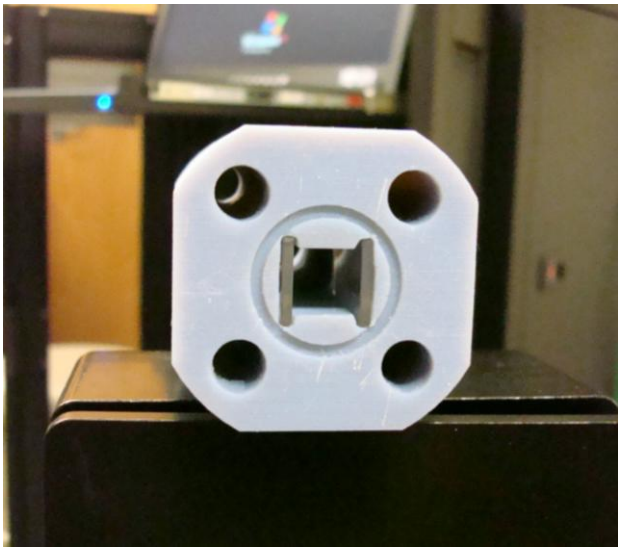

B.1- Quartz Containment

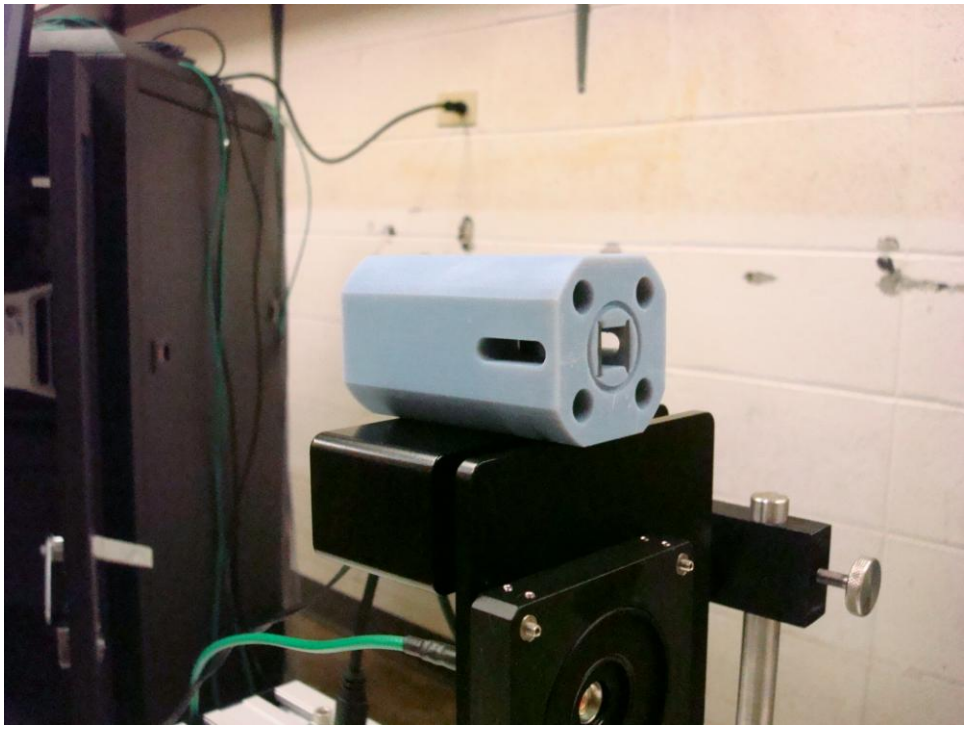

B.2- Quartz Containment

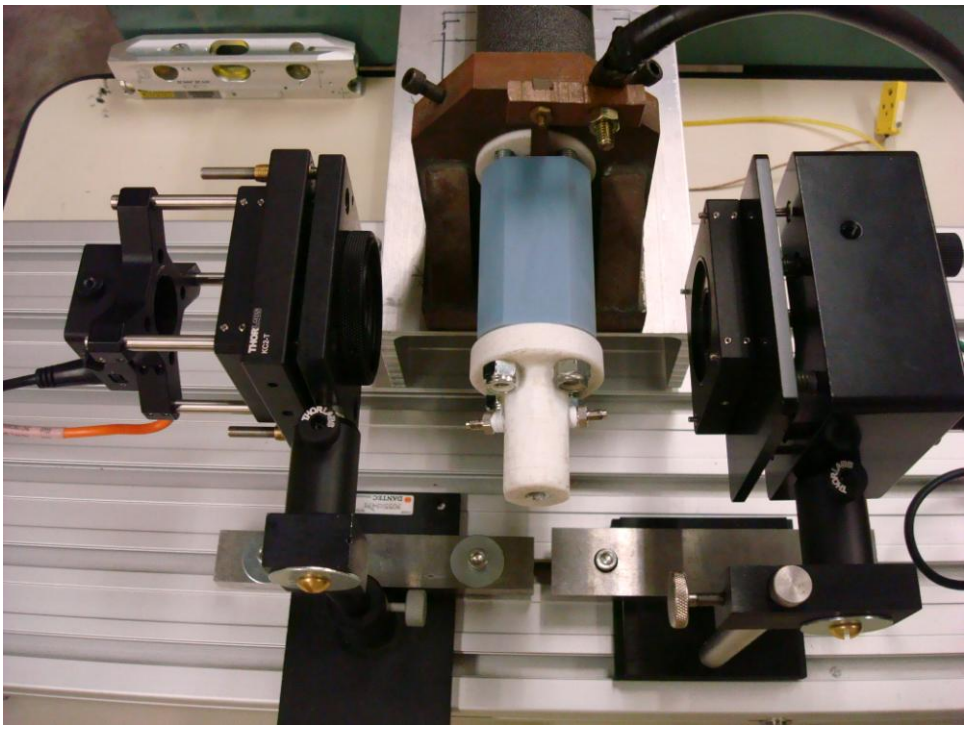

B.3- Test Setup

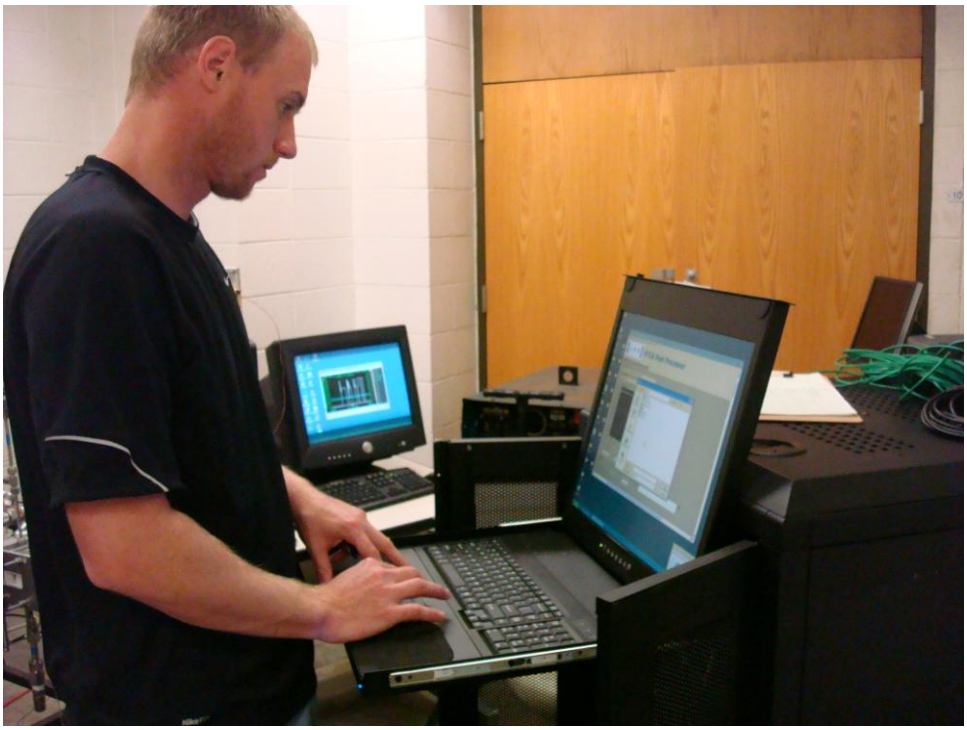

B.4- DAQ and TDLAS System

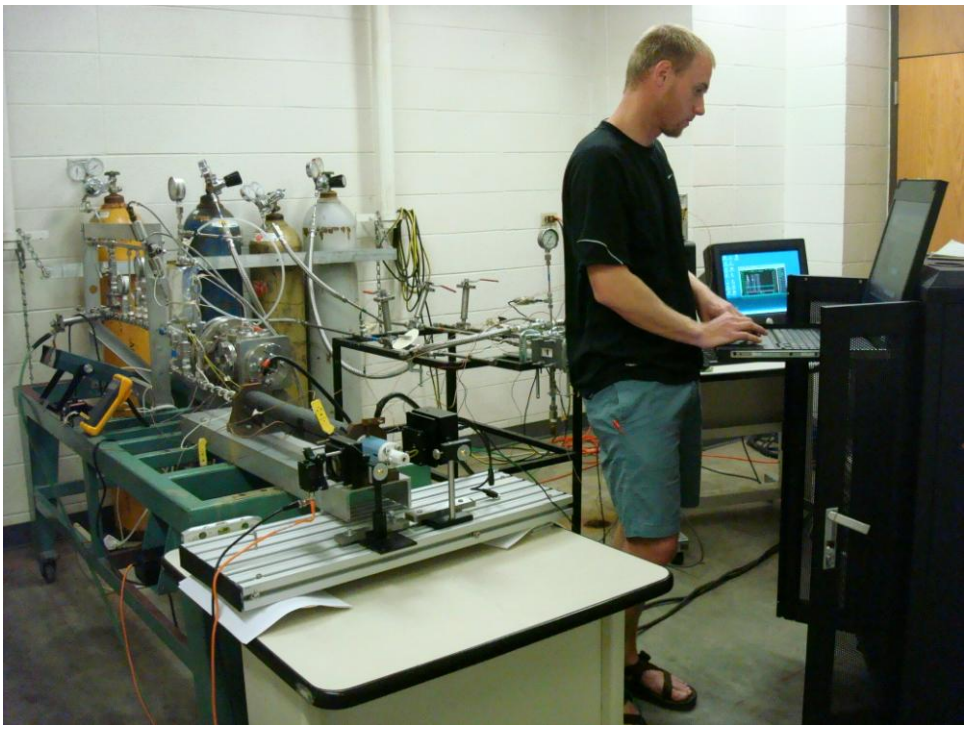

B.5 – Experimental Setup

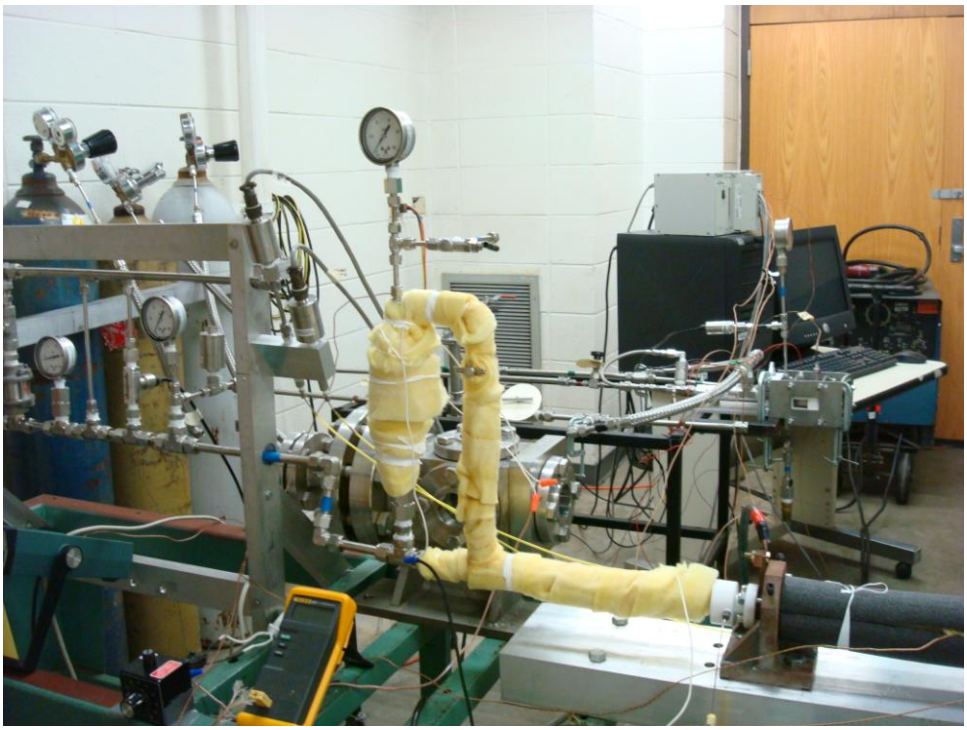

B.6 – Steam Injector

Appendix C

Rocket Motor Simulator Models

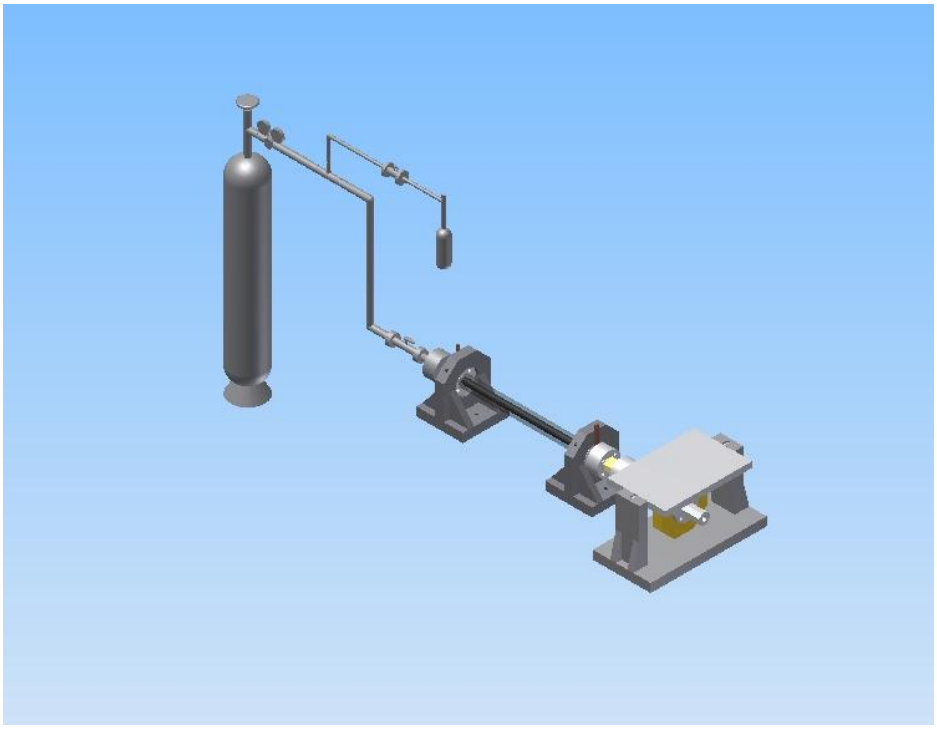

C.1 – 3D Model of HRS

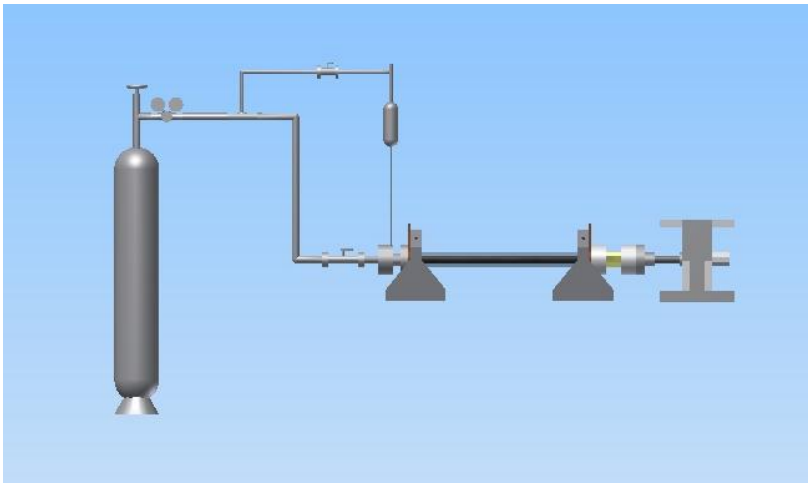

C.2 – 3D Model of HRS

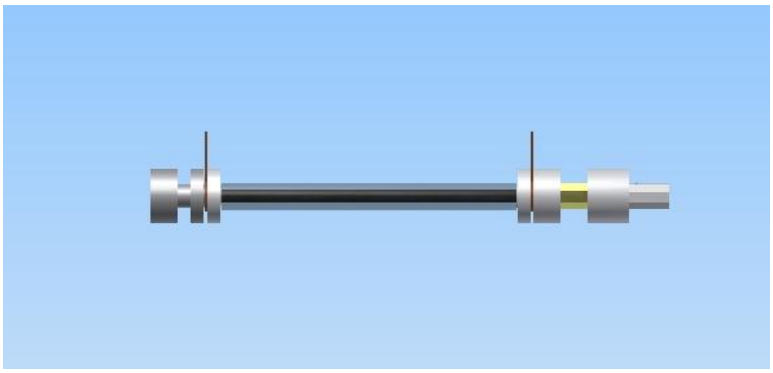

C.3 – 3D Model of Test Section

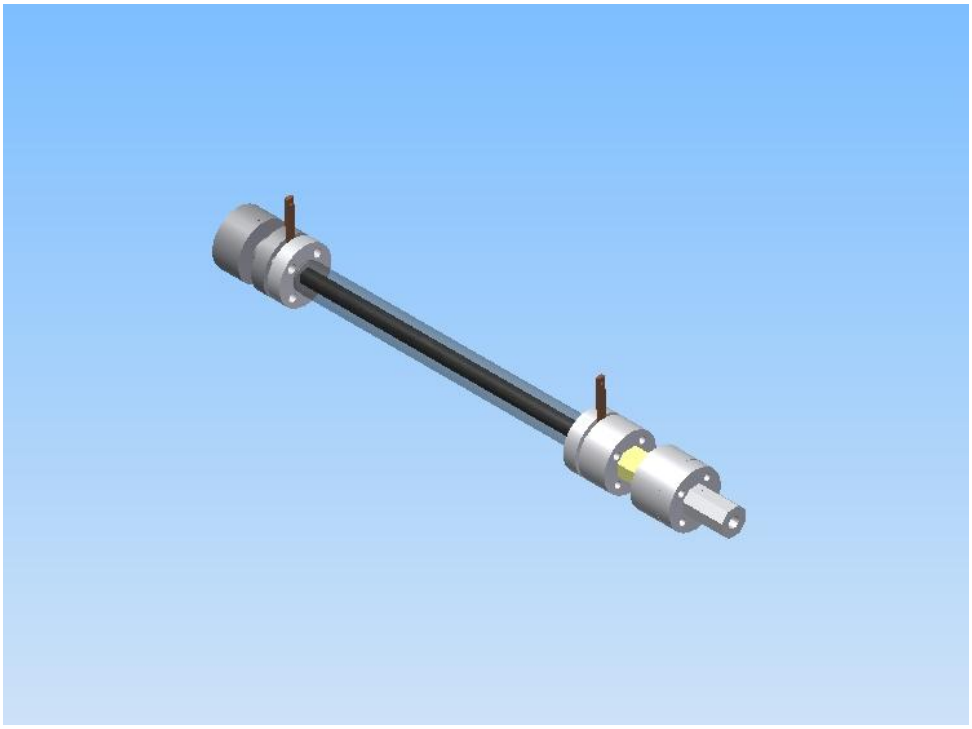

C.4 – 3D Model of Test Section

Appendix D

Rocket Motor Simulator Engineering Drawings

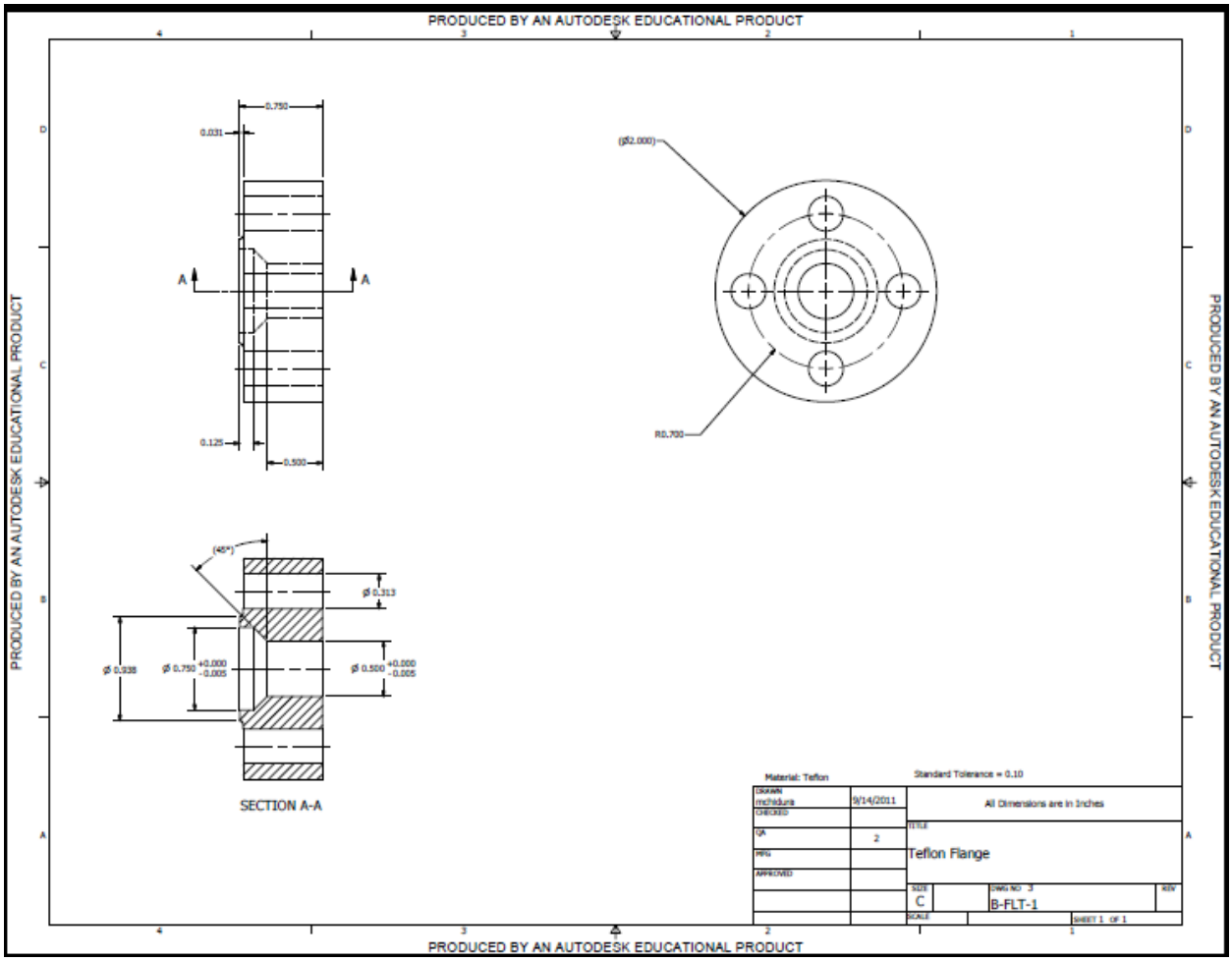

D.1 – Downstream Flange

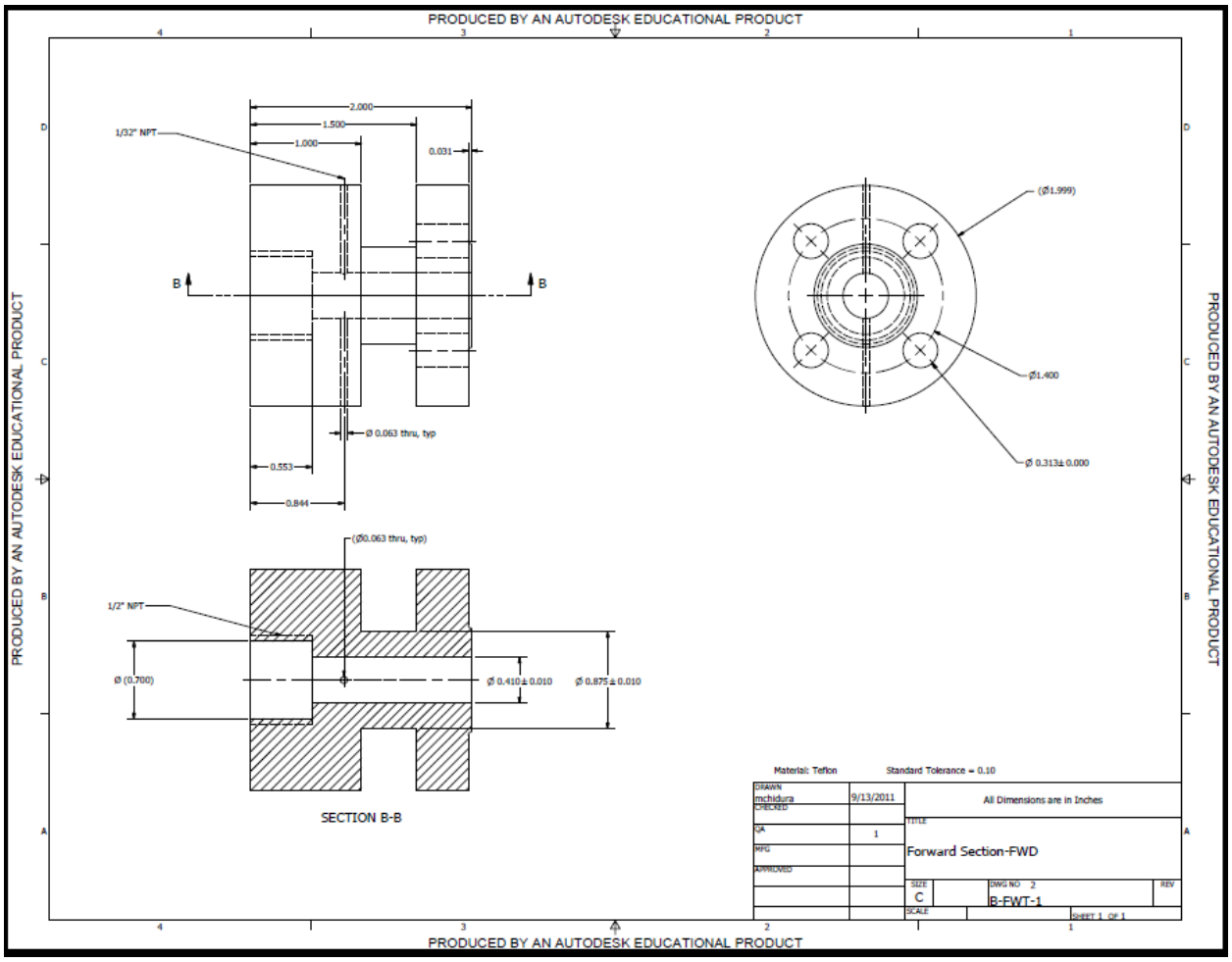

D.2 – Upstream Flange

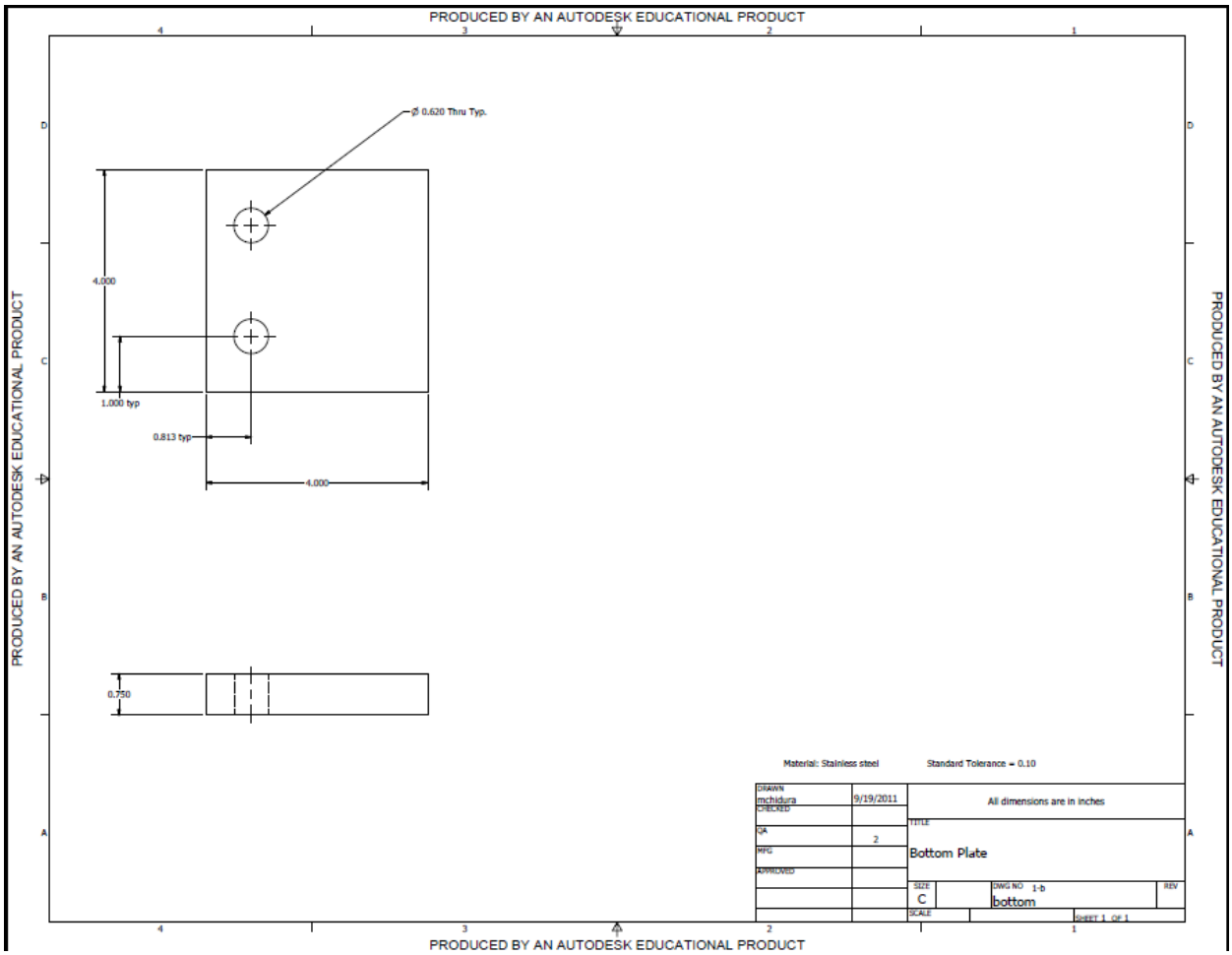

D.3 – Base Plate

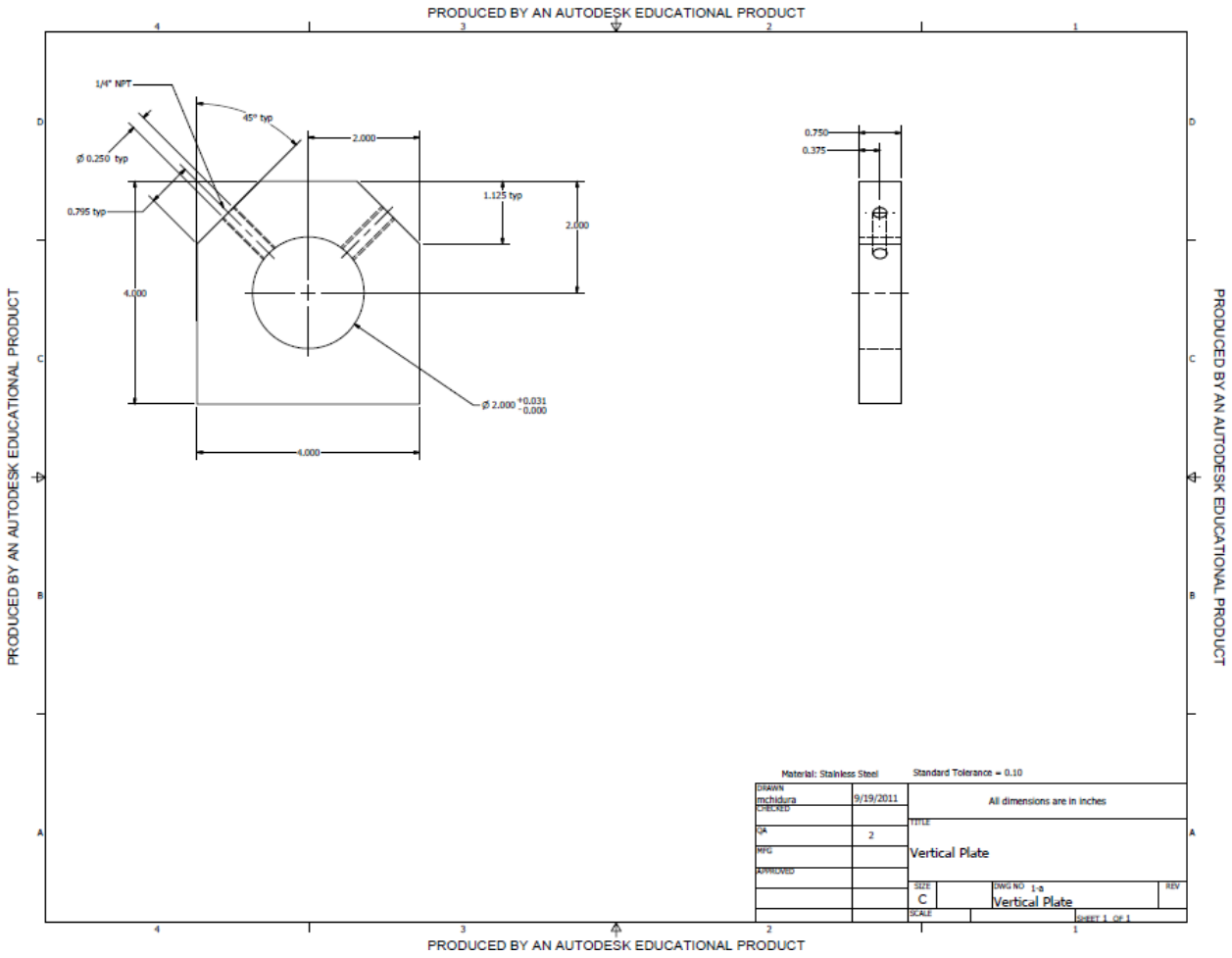

D.4 – Vertical Base Plate

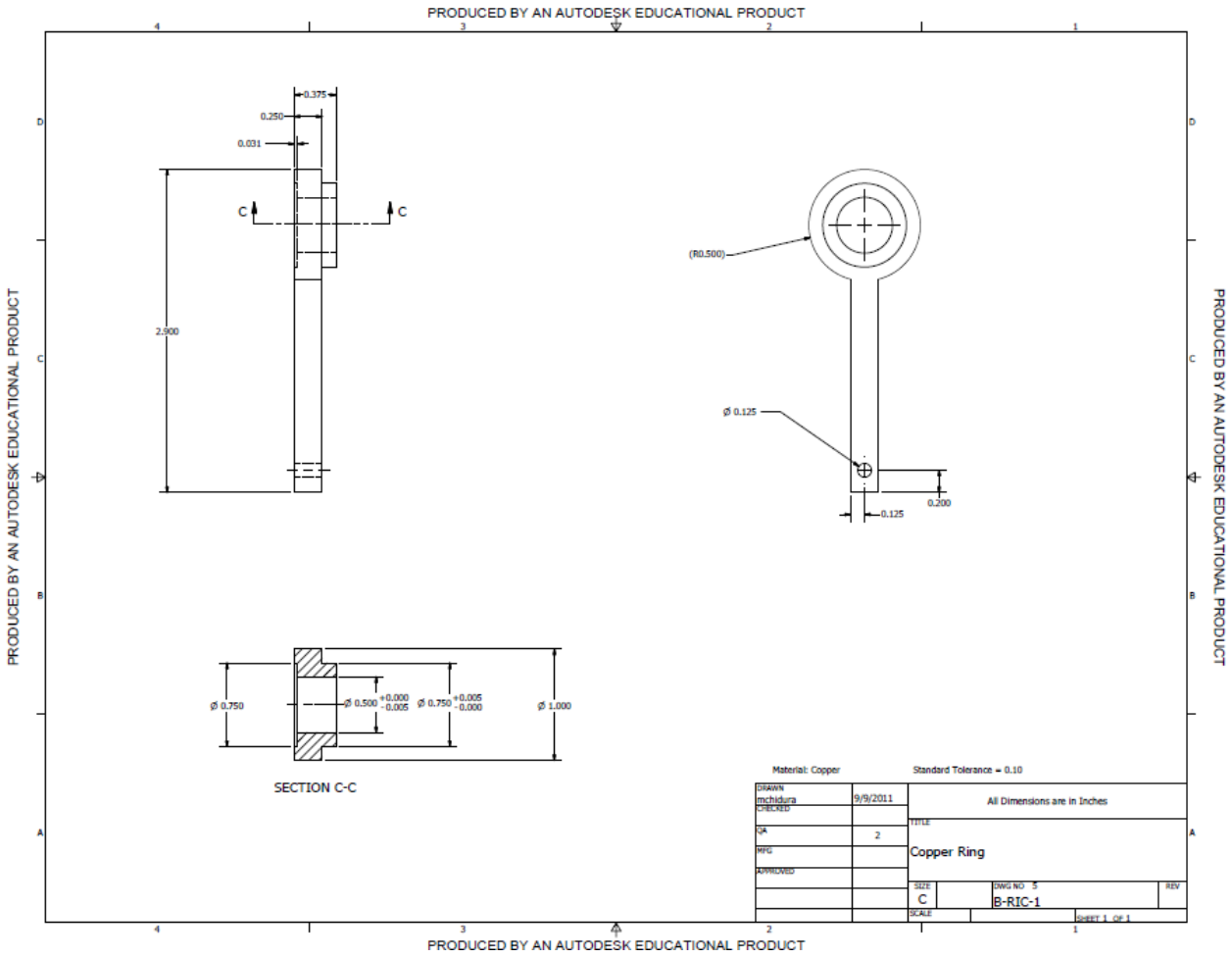

D.5 – Copper Electrode

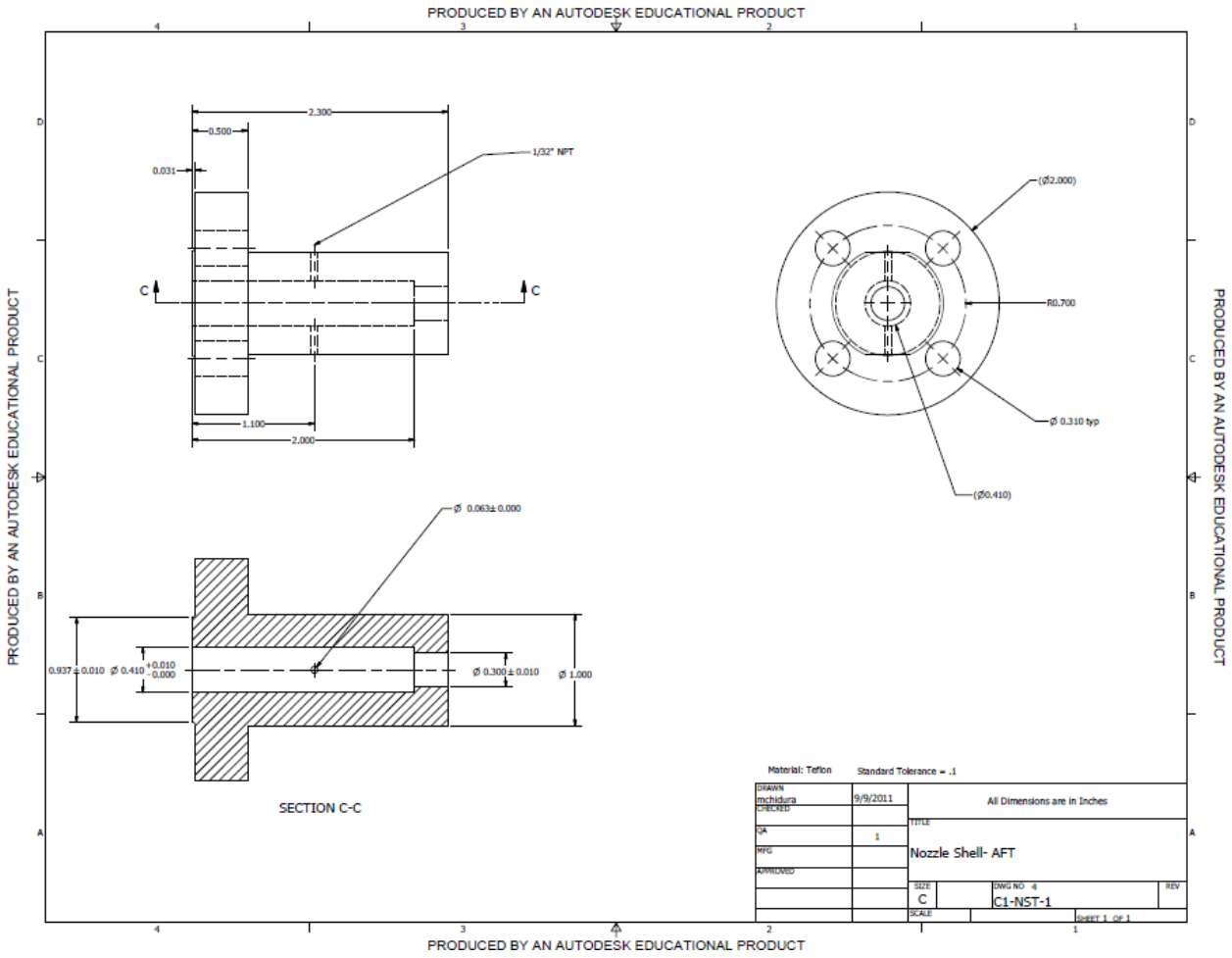

D.6- Exit Nozzle

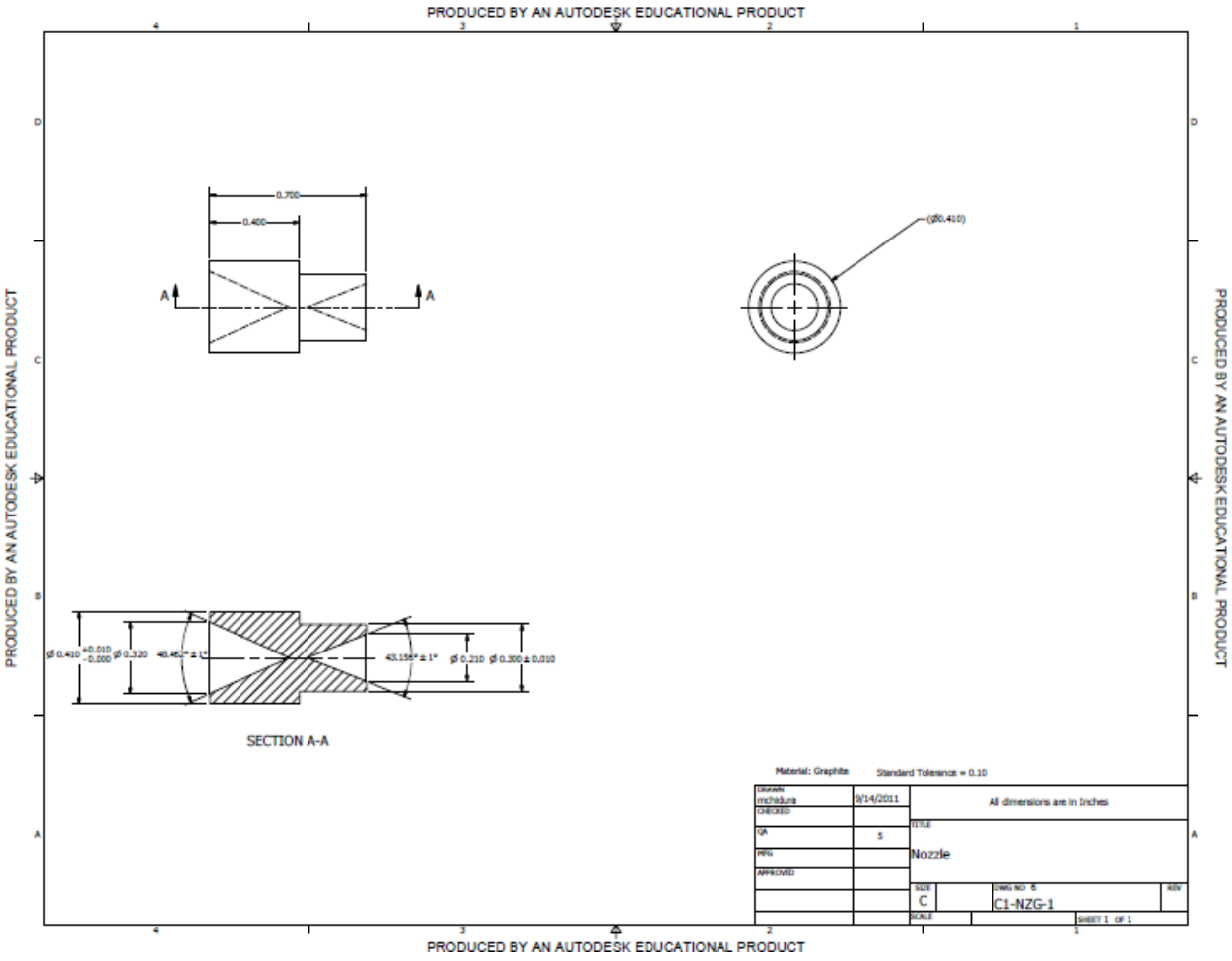

D.7- Graphite Nozzle

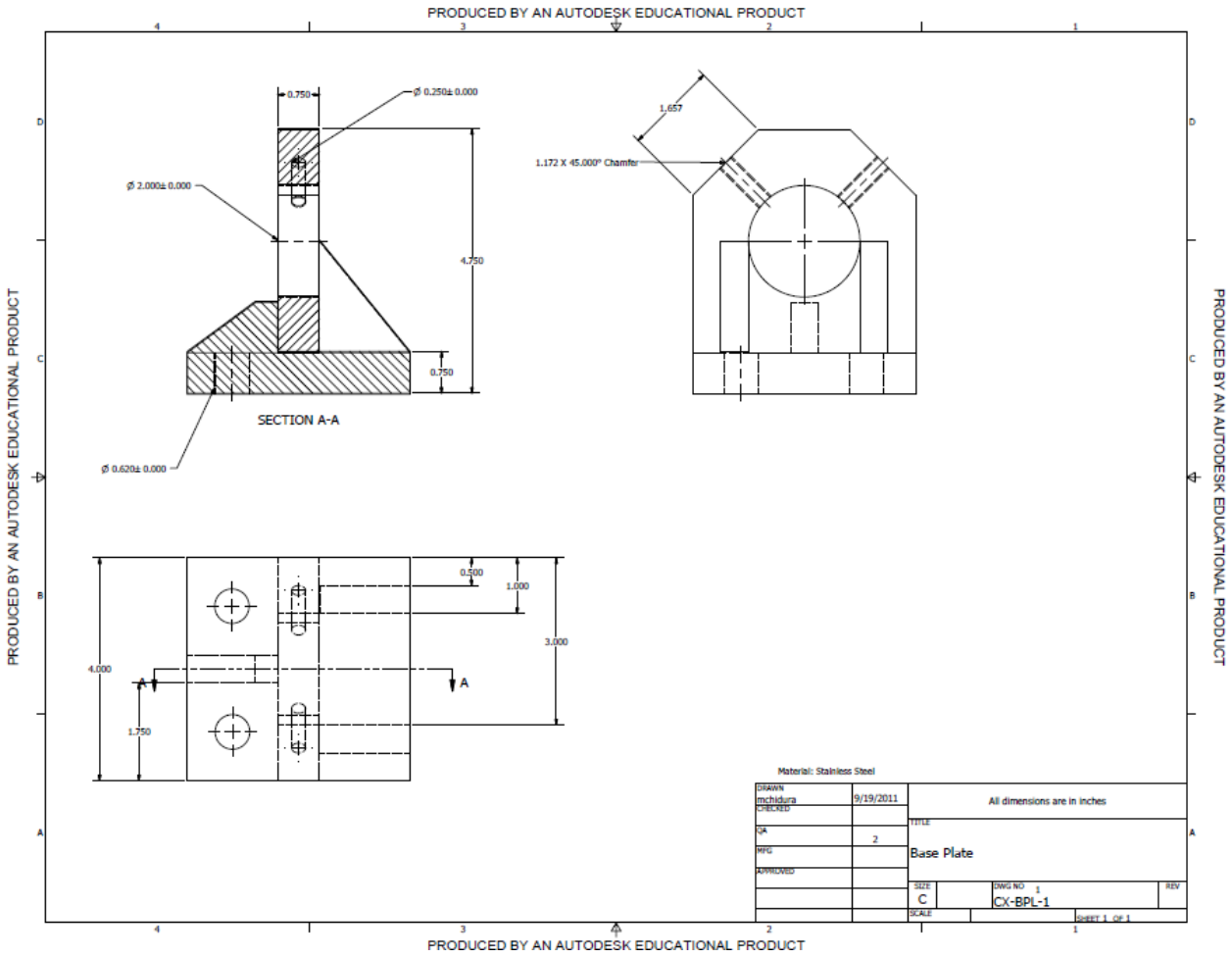

D.8 – Assembly of Base Plate

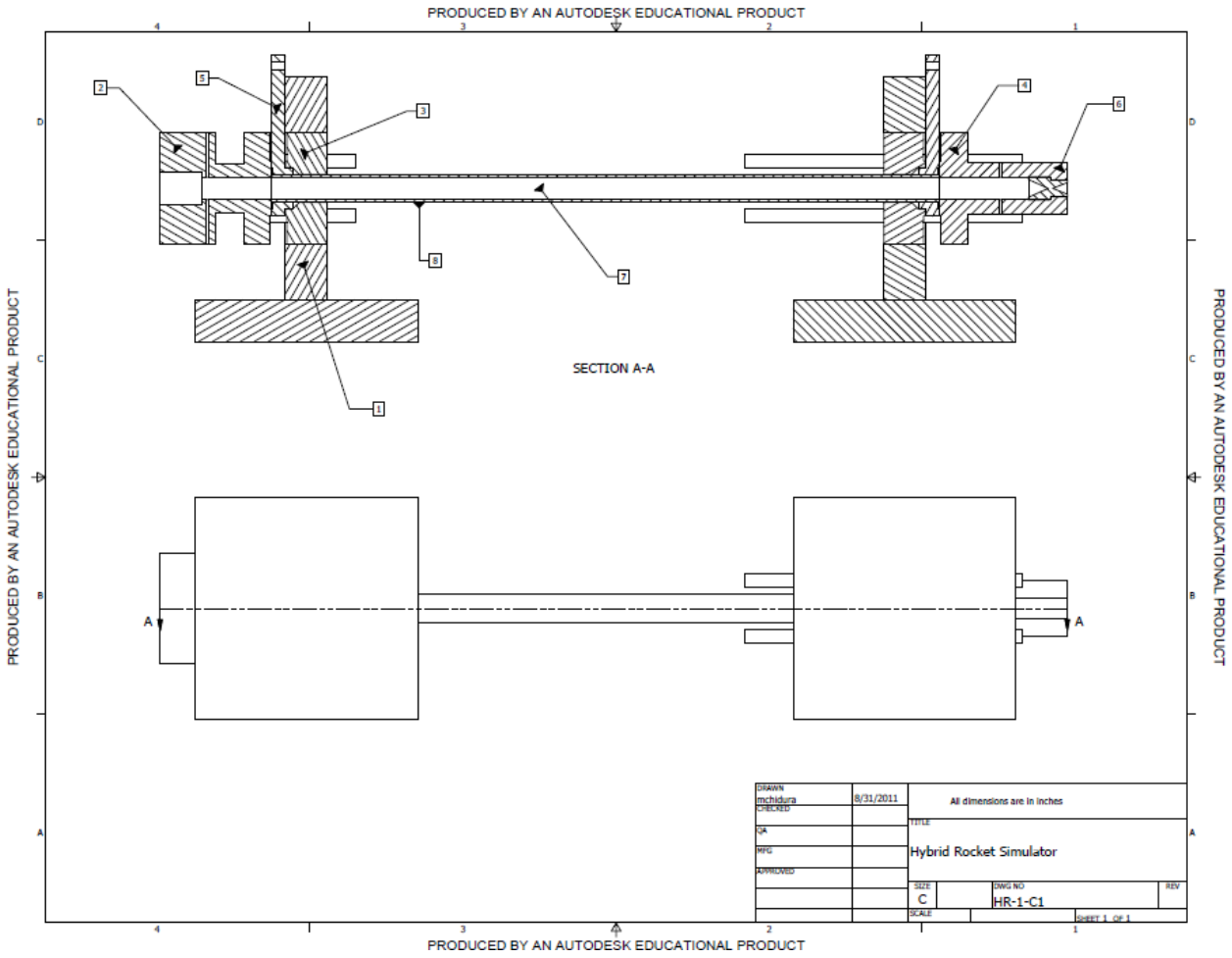

D.9 – Assembly of HRS

Appendix E

Instrument Calibration Curves

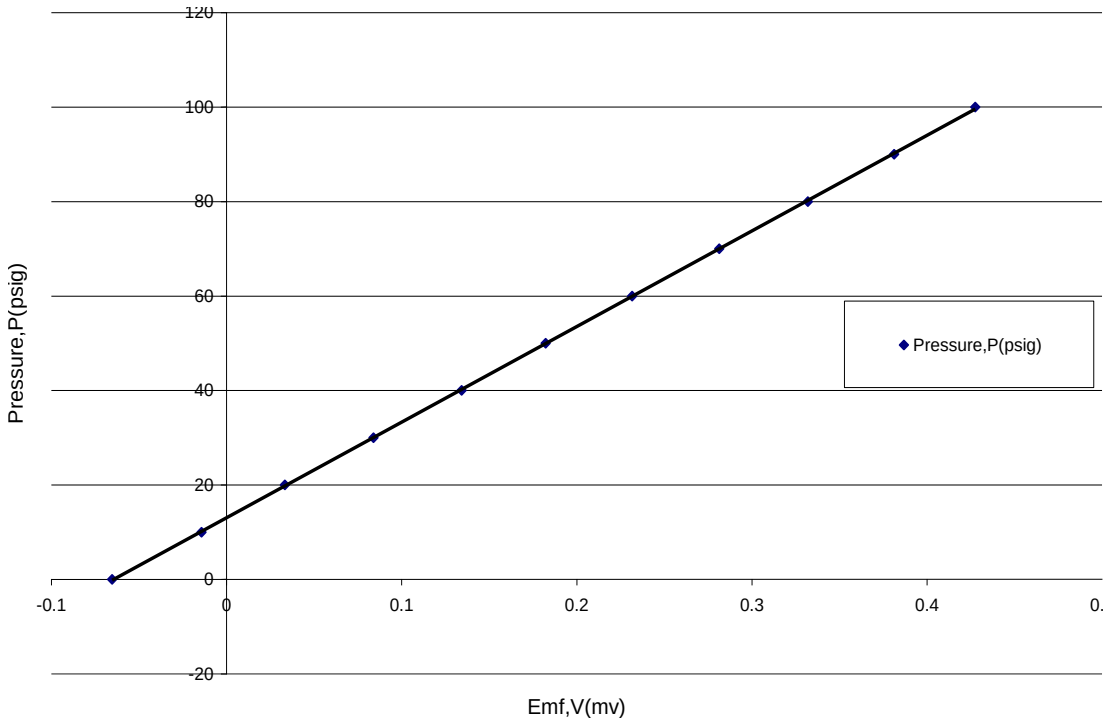

Figure E-1: Calibration curve for Upstream Pressure Transducer in Channel 1 of DAQ.

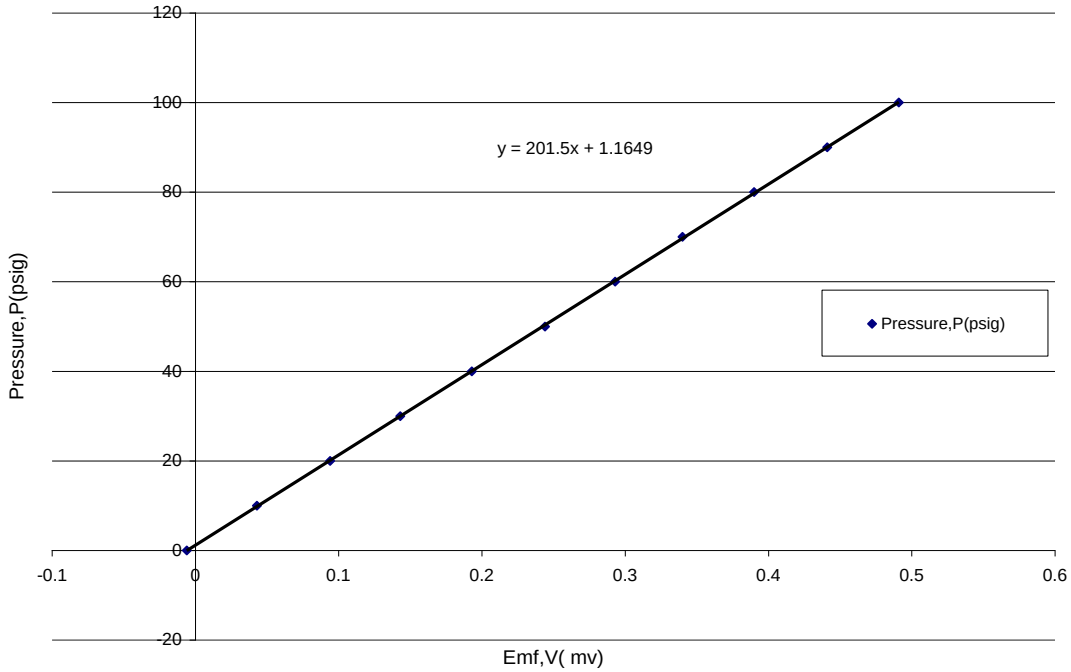

Figure E-2: Calibration Curve for Downstream Pressure Transducer in Channel 2 of DAQ.

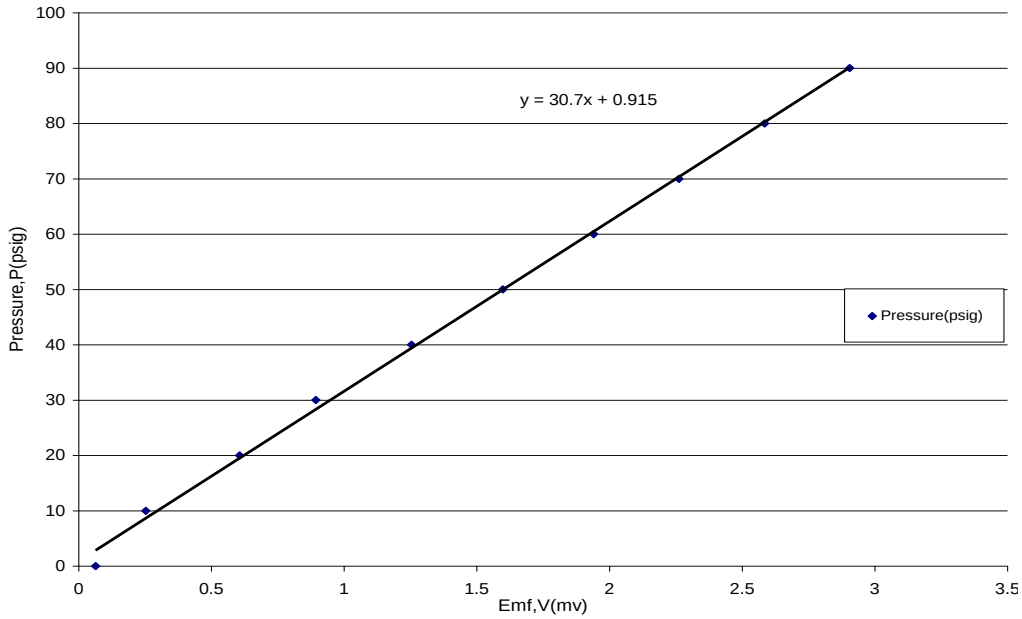

Figure E-3: Calibration Curve for Chamber Pressure Transducer in Channel 3 of DAQ.

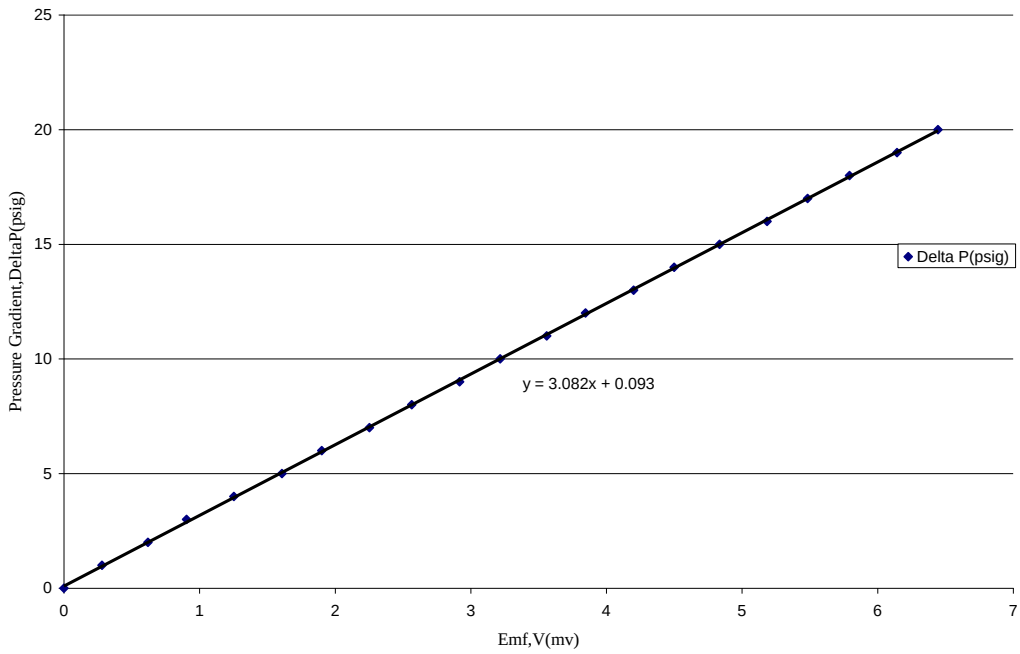

Figure E-4: Calibration Curve for Differential Pressure Transducer DAQ

Appendix F

Mass Flow Rate in Relation to Pressure Difference

The mass flow rate of the GOx across the orifice is measured by considering gaseous oxygen as a compressible fluid where the specific weight of the fluid changes as it flows through the orifice. The mass flow rate for such a flow is given by the following equation [32]

$$\dot{m} = KA_2\gamma_1 Y\sqrt{2g_0\left(\frac{P_1 - P_2}{\gamma_1}\right)} \tag{F.1}$$

where Y is expansion factor, K is flow coefficient.

The above equation was deduced to obtain the final equation for mass flow rate, which is given below

$$\dot{m} = \frac{1.87CA_2P_1g_c}{RT_1g_0\sqrt{1-\varepsilon^2}}\left[\left(1-\frac{\Delta P}{P_1}\right)^{1.4286}\left[\frac{1-\left(1-\Delta P/P_1\right)^{0.2857}}{1-\left(1-\Delta P/P_1\right)}\right]\times\left[\frac{1-\varepsilon^2}{1-\varepsilon^2\left(1-\Delta P/P_1\right)^{1.4286}}\right]\frac{2{g_0}^2\Delta PRT_1}{P_1g_c}\right]^{1/2} \tag{F.2}$$

where $\varepsilon = \frac{A_2}{A_1}$, A_2 is downstream area, $A_1$is upstream area.

Based on the above equation a relation between the pressure gradient and mass flow rate was established. This relation is given in the plot below.

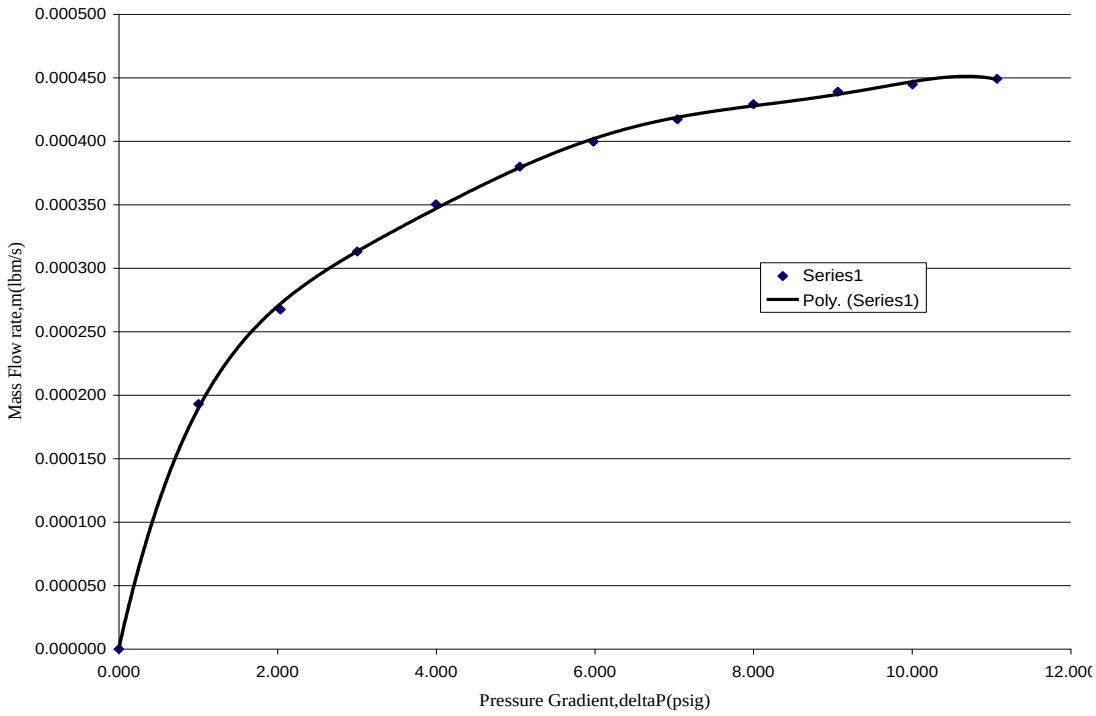

Figure F-1: Mass flow rate in relation to pressure gradient for the orifice.

Appendix G

Equipment List

Orifice Pressure Transducers:

Manufacturer: Omega

P/N: PX02C1-200GV

S/N: 135141 and 135147

Range: 0-200 psig

Chamber Pressure Transducer:

Manufacturer: Precise Sensors Inc.,

P/N: PX02C1-200GV

S/N: 25828

Range: 0-100 psig

Differential Pressure Transducer:

Manufacturer: Omega

P/N: PX821-010DV

S/N: 1503618

Range: 0-10 psid

DAQ Card:

Manufacturer: National Instruments

P/N: 18569A-01

Model: SCXI-1321

Thermocouples:

Manufacturer: Omega

P/N: GG-K-24-SLE

Material: + Yellow (Chromega) – Red (Alomega)

Deviation of Thermocouples: -1.4 °F at 800.0 °F

Pressure Gauges:

Manufacturer: Matheson

P/N: 63-2212

Ball Valves:

Manufacturer: Worcester

P/N: ½ in C466PMSE R60

Working Pressure: 1500 psig

Meter Valve:

Manufacturer: Whitey

P/N: ¼ in SS 31RS4

Software:

National Instruments Virtual Bench Version 2.6.2

NI-DAQ 6.9

TDLAS:

Los Gatos Research High Temperature Gas Analyzer

Vita

The author was born in Lafayette, Louisiana. He obtained his Bachelor's degree in Mechanical Engineering from the University of Colorado at Colorado Springs. He has previously conducted research on ablation rates in stainless steel pipes for high temperature hydrogen flow at the University of New Orleans.